method (Microtrack UPA150; Nikkiso, Tokyo, Japnan). A sample of nanoparticulate suspension in distilled water was used for particle size analysis. The diameter of PLGA NP was 196 ± 29 nm. Surface charge (zeta potential) was also analyzed by Zetasizer Nano (Sysmex, Hyogo, Japan) and was anionic charge (-15±10 mV at pH 4.4).

Scanning electron microscopy (SEM) image

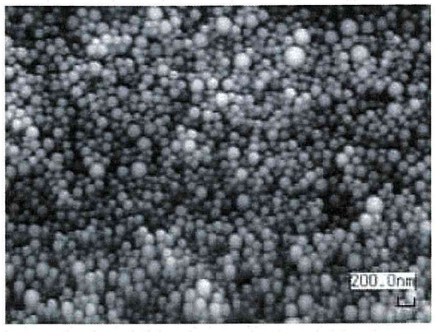

Particle size distribution of FITC-incorporated PLGA nanoparticles in water

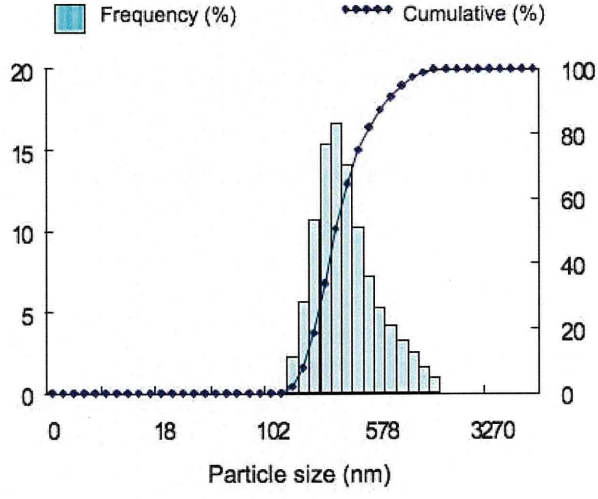

Bioabsorption process of PLGA NP

The chemical structure of PLGA and its bioabsorption process (hydrolysis) are indicated below. Scanning electron microscopic examination of time course of biodegradation in phosthe phate buffer solution shows slow degradation of NP with time.

Bioabsorption Process (hydrolysis) of PLGA

Chemical structure of PLGA and its hydrolysis process in living body

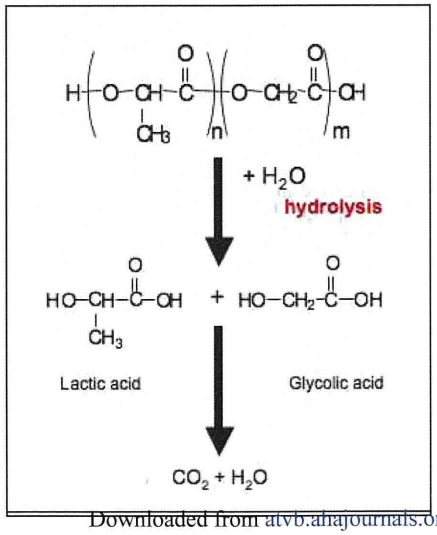

Biodegradation of PLGA nanoparticles (a mean diameter: 200 nm) in phosphate buffer solution (pH 7.4, 32°C)

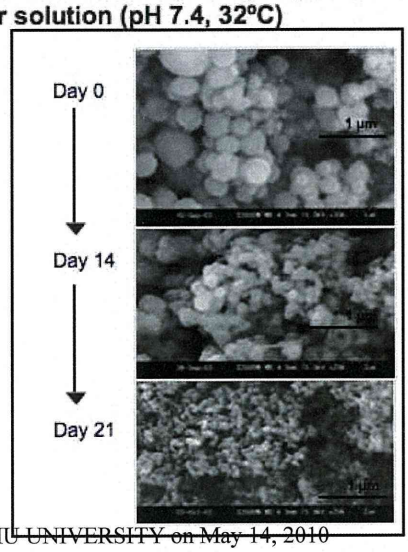

Intracellular uptake and intracellular distribution of NPs

Human umbilical vein endothelial cells (HUVEC) were obtained from Cambrex BioScience Walkersville, Inc., cultured in EGM-2 (Lonza, Charles City, IA) with supplements (Lonza), and used between passages 4 to 8. Human skeletal muscle cells (SkMC) were also obtained from Cambrex BioScience Walkersville, Inc. and cultured in SkGM (Lonza).

The HUVEC and SkMC were seeded on the 8-well-chamber slide to an initial concentration of 1.5×10^4 cells per well and incubated at 37 °C/5 % CO_2 environment until cells were subconfluent. The growth medium was replaced with the FITC-NP suspension medium (0.1 to 0.5 mg/ml) without supplements and then further incubated for 1 hour. The cells were then washed three times with PBS to eliminate extracellular NP as previously described[4]. Then, the cells were fixed with methyl-alcohol and nuclei were counterstained with propidium iodide (PI; vector shield). Intracellular uptake of FITC-NP was evaluated by fluorescence microscopy (Biozero; KEYENCE, Osaka, Japan). The number of cells in 5 random fields was manually counted and cellular uptake percentage was assessed by the percentage of fluorescence positive cells per total cells.

In another set of experiments using HUVEC, the growth medium was replaced with FITC-NP (0.5 mg/ml) and further incubated for 1 hour. After excess extracellular NP were washed with PBS, the cells were cultured with normal growth medium and intracellular retention of FITC was examined as described above at days 3 and 7.

To investigate the potential mechanism of cellular uptake of NP, HUVEC and SkMC were seeded on the 96-well plate in the presence or absence of an inhibitor of clathrin-mediated endocytosis pathway[5], chlorpromazine (CPZ; Sigma) at 10 or 30 μM for 30 min at 37 °C in the culture medium without supplements, and then incubated with FITC-NP suspension medium (0.1 to 0.5 mg/ml) for further 30 min. After incubation, cells were washed and lysed with triton X and NaOH and then the amount of fluorescence in each wells were analyzed with fluorescence-plate reader (Mithras LB940; BERTHOLD BIOTECHNOLOGY, Germany).

Angiogenesis Assay of Human Endothelial Cell

Angiogenesis assay of human endothelial cells was tested by 2-dimensional Matrigel assay as previously described.[6] HUVECs (2×10^4) were suspended on the 8-well-chamber slide pre-coated with 200 μl Matrigel (BD Bioscience) in 500 μl EBM-2 medium with supplements (Lonza) in the presence or absence of pitavastatin or NP incorporated with pitavastatin at 1 and 10 nM. In another set of experiments, HUVEC were pre-treated with pitavastatin or NP incorporated with pitavastatin at 1 and 10 nM for 24 hours and washed, and then the cells were suspended on the Matrigel.

After 24 hours of incubation on the Matrigel at 37 °C/5 % CO_2 environment, tube formation were quantified by light microscopy (Biozero; KEYENCE, Osaka, Japan) and the length of completed tube-like structures in 5 random fields was quantified in a blinded fashion in each expreiment.

Animal Preparation and Experimental Protocol

The study protocol was reviewed and approved by the Committee on Ethics on Animal Experiments, Kyushu University Faculty of Medicine, and the experiments were conducted according to the Guidelines of the American Physiological Society.

Male 8-weeks-old C57BL/6J wild-type mice (Japan-Clea, Tokyo, Japan) were bred and maintained in the Laboratory of Animal Experiments at Kyushu University. After anesthesia with an intraperitoneal injection of ketamine hydrochloride (70 mg/kg) and

xyladine hydrochloride (3 mg/kg), we induced unilateral hindlimb ischemia to mice as previously described.[7, 8] Briefly, the proximal portion of the left femoral artery and vein including the superficial and deep branch as well as the distal portion of saphenous artery and vein were ligated and resected after all side branches were dissected free. Immediately after induction of ischemia, animals were randomly divided into 4 groups; a control no treatment group and others received intramuscular injections of FITC-NP (PLGA at 0.18 mg/100 μl) (NP group), intramuscular injections of pitavastatin at 0.01 mg/100 μl (0.4 mg/kg)(Pitava only group), or intramuscular injections of pitavastatin-NP [PLGA at 0.18 mg/100 μl containing 0.01 mg (0.4 mg/kg) of pitavastatin] (Pitava-NP group) into the left femoral and thigh muscles with a 27-gauge needle. This dose of pitavastatin NP was selected because we examined effects of pitavastatin-NP containing pitavastatin at 0.1, 0.4, 1.0 and 1.5 mg/kg 1n preliminary studies and confirmed that pitavastatin NP containing 0.4 mg/kg pitavastatin was an optimal dose in our experiments. Biochemical parameters listed in supplemental Table 1 were measured 3, 7, and 14 days after treatment.

In another set of experiments, effects of intramuscular injections of pitavastatin-NP were examined in $eNOS^{-/-}$ mice and wild-type mice chronically treated with *N*ω-nitro-L-arginine methyl ester (L-NAME; Sigma), an NO synthase inhibitor, in drinking water (2 mg/kg) from 7 days before operation to sacrifice[9]. Two other groups received intramuscular injections of non-nanoparticulated soluble pitavastatin at high doses at 4 and 20 mg/kg. Furthermore, three other groups received systemic daily oral administration of pitavastatin at doses of 0.4, 1.0 and 10 mg/kg, solved in 0.5 % carboxymethyl cellulose by gavage from the day of surgery until the mice were sacrifice on day 14.

Histological and immunohistochemical analyses

Histological evaluation was performed in 5-μm paraffin embedded sections from gastrocnemius muscle 14 days after hindlimb ischemia. Capillary and arteriolar density in ischemic muscle were determined by immunohistochemical staining with anti-mouse platelet endothelial cell adhesion molecule (PECAM)-1 antibody (CD31; Santa Cruz Biotechnology) and α-smooth muscle actin (α-SMA; DAKO), respectively. Digital images of 5 microscopic fields from 4 different sections from each animal were stored. Capillary density was expressed as the number of CD31 positive cells per mm^2 and arteriolar density was expressed as the number of circumvented brown signals of α-SMA per mm^2 as previously described[10]. To determine intracellular molecular signals for angiogensis, cross sections were stained with anti-phosphorylated-Akt antibody (Cell Signaling) or anti-phosphorylated-eNOS antibody (Cell Signaling)[9]. To determine cellular localization of angiogenic growth factors 3, 7 and 14 days after ischemia, cross sections were stained with anti-VEGF or anti-FGF-2 antibody with anti-PECAM-1 (CD31) antibody, as a primary antibody (all from Santa Cruz Biotechnology), and anti-mouse IgG (Alexa 488; Molecular Probes) or anti-rabbit IgG (FITC; Santa Cruz Biotechnology) with anti-goat IgG antibody (Alexa 555; Molecular Probes), as a secondary antibody, respectively. Nuclei were counterstained with 4', 6-diamidino-2-phenylindole (DAPI; Vector Shield).

Distribution of nanoparticles *in vivo*

Three, 7 and 14 days after hindlimb ischemia and intramuscular injection of FITC-NP, gastrocnemius muscle was isolated from ischemic and non-ischemic limbs, and FITC signals were examined under a fluorescent stereomicroscope. Frozen cross sections of those muscles were then prepared and examined under a fluorescent microscope (Biozero, KEYENCE, Osaka, Japan). Nuclei were counterstained with propidium iodide (PI; Vector Shield). Another sections were stained with anti-mouse PECAM-1 antibody (CD31; Santa

Cruz Biotechnology), as a primary anti-body, and anti-goat IgG (Alexa 555; Molecular Probes), as a secondary anti-body. Frozen cross sections of liver, spleen and kidney were also examined.

Western blotting

Homogenates of muscle tissues were analyzed for immunoblotting 7 days after induction of hindlimb ischemia. Proteins were separated in 7.5 % or 15 % SDS-polyacrylamide gels and then blotted onto a membrane. Membrane was incubated with antibodies against phosphorylated-Akt, phosphorylated-eNOS, Akt (1:1000, Cell Signaling), eNOS (1:1000, Affinity BioReagents), VEGF, FGF-2 and MCP-1 (1:200, Santa Cruz Biotechnology) and then the blots were reprobed with GAPDH (1:1000, Santa Cruz Biotechnology).

Flow Cytometric Analyses of EPC Mobilization

Peripheral blood was obtained from mice 7 and 14 days after hindlimb ischemia. EPC are thought to derive from mononuclear leukocytes that are positive for both Sca-1 and Flk-1 (vascular endothelial cell growth factor receptor-2)[11, 12]. The percentage of mononuclear cells that were positive for both the Sca-1-FITC and Flk-1-PE antibodies (Pharmingen) was then analyzed with a FACS Caliber flow cytometer (Becton Dickinson).

Measurements of statin concentration in serum and muscle tissue

Statin concentration in serum and muscle were measured at predetermined time points by using column-switching high performance liquid chromatography (HPLC) system as previously reported[13]. Briefly, the column-switching HPLC system consists of two LC-10AD pumps, an SIL-10A auto-sampler, a CTO-10A column oven, a six-port column-switching valve and an SPD-10A UV-detector (all from Shimadzu, Kyoto, Japan). The column temperature was maintained at 40 °C. Preprepared serum or tissue homozynates sample solutions were injected from auto-sampler into HPLC system and the detection of statin in sample solutions was carried out at 250 nm with a UV-detector. The detected peak-area was measured with Lcsolution software (Shimadzu, Kyoto, Japan).

References

1. Okada H, Inoue Y, Heya T, Ueno H, Ogawa Y, Toguchi H. Pharmacokinetics of once-a-month injectable microspheres of leuprolide acetate. *Pharm Res.* 1991;8:787-791.
2. Kawashima Y, Yamamoto H, Takeuchi H, Hino T, Niwa T. Properties of a peptide containing DL-lactide/glycolide copolymer nanospheres prepared by novel emulsion solvent diffusion methods. *Eur J Pharm Biopharm.* 1998;45:41-48.
3. Kawashima Y, Yamamoto H, Takeuchi H, Fujioka S, Hino T. Pulmonary delivery of insulin with nebulized DL-lactide/glycolide copolymer (PLGA) nanospheres to prolong hypoglycemic effect. *J Control Release.* 1999;62:279-287.
4. Kimura S, Egashira K, Nakano K, Iwata E, Miyagawa M, Tsujimoto H, Hara K, Kawashima Y, Tominaga R, Sunagawa K. Local delivery of imatinib mesylate (STI571)-incorporated nanoparticle ex vivo suppresses vein graft neointima formation. *Circulation.* 2008;118:S65-70.
5. Kanatani I, Ikai T, Okazaki A, Jo J, Yamamoto M, Imamura M, Kanematsu A, Yamamoto S, Ito N, Ogawa O, Tabata Y. Efficient gene transfer by pullulan-spermine occurs through both clathrin- and raft/caveolae-dependent mechanisms. *J Control Release.* 2006;116:75-82.
6. Weis M, Heeschen C, Glassford AJ, Cooke JP. Statins have biphasic effects on

angiogenesis. *Circulation.* 2002;105:739-745.

7. Aicher A, Heeschen C, Mildner-Rihm C, Urbich C, Ihling C, Technau-Ihling K, Zeiher AM, Dimmeler S. Essential role of endothelial nitric oxide synthase for mobilization of stem and progenitor cells. *Nat Med.* 2003;9:1370-1376.
8. Urbich C, Heeschen C, Aicher A, Dernbach E, Zeiher AM, Dimmeler S. Relevance of monocytic features for neovascularization capacity of circulating endothelial progenitor cells. *Circulation.* 2003;108:2511-2516.
9. Hiasa K, Ishibashi M, Ohtani K, Inoue S, Zhao Q, Kitamoto S, Sata M, Ichiki T, Takeshita A, Egashira K. Gene transfer of stromal cell-derived factor-1alpha enhances ischemic vasculogenesis and angiogenesis via vascular endothelial growth factor/endothelial nitric oxide synthase-related pathway: next-generation chemokine therapy for therapeutic neovascularization. *Circulation.* 2004;109:2454-2461.
10. Masaki I, Yonemitsu Y, Yamashita A, Sata S, Tanii M, Komori K, Nakagawa K, Hou X, Nagai Y, Hasegawa M, Sugimachi K, Sueishi K. Angiogenic gene therapy for experimental critical limb ischemia: acceleration of limb loss by overexpression of vascular endothelial growth factor 165 but not of fibroblast growth factor-2. *Circ Res.* 2002;90:966-973.
11. Landmesser U, Engberding N, Bahlmann FH, Schaefer A, Wiencke A, Heineke A, Spiekermann S, Hilfiker-Kleiner D, Templin C, Kotlarz D, Mueller M, Fuchs M, Hornig B, Haller H, Drexler H. Statin-induced improvement of endothelial progenitor cell mobilization, myocardial neovascularization, left ventricular function, and survival after experimental myocardial infarction requires endothelial nitric oxide synthase. *Circulation.* 2004;110:1933-1939.
12. Iwakura A, Shastry S, Luedemann C, Hamada H, Kawamoto A, Kishore R, Zhu Y, Qin G, Silver M, Thorne T, Eaton L, Masuda H, Asahara T, Losordo DW. Estradiol enhances recovery after myocardial infarction by augmenting incorporation of bone marrow-derived endothelial progenitor cells into sites of ischemia-induced neovascularization via endothelial nitric oxide synthase-mediated activation of matrix metalloproteinase-9. *Circulation.* 2006;113:1605-1614.
13. Kojima J, Fujino H, Yosimura M, Morikawa H, Kimata H. Simultaneous determination of NK-104 and its lactone in biological samples by column-switching high-performance liquid chromatography with ultraviolet detection. *J Chromatogr B Biomed Sci Appl.* 1999;724:173-180.

Nanoparticle-Mediated Delivery of Nuclear Factor κB Decoy Into Lungs Ameliorates Monocrotaline-Induced Pulmonary Arterial Hypertension

Satoshi Kimura, Kensuke Egashira, Ling Chen, Kaku Nakano, Eiko Iwata, Miho Miyagawa, Hiroyuki Tsujimoto, Kaori Hara, Ryuichi Morishita, Katsuo Sueishi, Ryuji Tominaga, Kenji Sunagawa

Abstract—Pulmonary arterial hypertension (PAH) is an intractable disease of the small pulmonary artery that involves multiple inflammatory factors. We hypothesized that a redox-sensitive transcription factor, nuclear factor κB (NF-κB), which regulates important inflammatory cytokines, plays a pivotal role in PAH. We investigated the activity of NF-κB in explanted lungs from patients with PAH and in a rat model of PAH. We also examined a nanotechnology-based therapeutic intervention in the rat model. Immunohistochemistry results indicated that the activity of NF-κB increased in small pulmonary arterial lesions and alveolar macrophages in lungs from patients with PAH compared with lungs from control patients. In a rat model of monocrotaline-induced PAH, single intratracheal instillation of polymeric nanoparticles (NPs) resulted in delivery of NPs into lungs for ≤14 days postinstillation. The NP-mediated NF-κB decoy delivery into lungs prevented monocrotaline-induced NF-κB activation. Blockade of NF-κB by NP-mediated delivery of the NF-κB decoy attenuated inflammation and proliferation and, thus, attenuated the development of PAH and pulmonary arterial remodeling induced by monocrotaline. Treatment with the NF-κB decoy NP 3 weeks after monocrotaline injection improved the survival rate as compared with vehicle administration. In conclusion, these data suggest that NF-κB plays a primary role in the pathogenesis of PAH and, thus, represent a new target for therapeutic intervention in PAH. This nanotechnology platform may be developed as a novel molecular approach for treatment of PAH in the future. (***Hypertension.* 2009;53:877-883.**)

Key Words: pulmonary hypertension ■ lung ■ inflammation ■ leukocytes

Pulmonary arterial hypertension (PAH) is an intractable disease of the small pulmonary arteries that results in a progressive increase in pulmonary vascular resistance, right ventricular failure, and, ultimately, premature death.[1–3] Because its mortality remains high even after the introduction of prostacyclin infusion therapy (which has raised the 5-year survival rate to ≈50%), the development of a more effective and less invasive therapy for PAH is urgently needed.

Recent evidence suggests an important role of monocyte chemoattractant protein (MCP) 1–mediated inflammation in the mechanism of PAH.[4–8] However, the therapeutic benefits of MCP-1 blockade were not optimal for clinical application.[5,6] During the inflammatory process of PAH, several inflammatory factors (eg, MCP-1, interleukin [IL] 1, IL-6, and tumor necrosis factor [TNF] α) are overproduced, leading to a vicious circle.[1–3] A redox-sensitive transcription factor, nuclear factor κB (NF-κB), is known to regulate expression of chemokines such as MCP-1 and multiple inflammatory cytokines such as IL-6 and TNF-α. Blockade of NF-κB by transfection of NF-κB "decoy" oligodeoxynucleotides may attenuate the vascular pathology associated with reduced expression of NF-κB–dependent genes.[9–12] However, no previous study has addressed the specific role of the NF-κB pathway in the pathogenesis of PAH. Therefore, we hypothesized that controlled local delivery of NF-κB decoy into lungs, targeting a battery of multiple important inflammatory cytokines, would be a favorable therapeutic approach for PAH. To this end, we have recently developed bioabsorbable polymeric nanoparticles (NPs) formulated from a poly-(ethylene glycol)-*block*-lactide/glycolide copolymer (PEG-PLGA).[13–15]

The primary aim of this study was to investigate the role of the NF-κB pathway in the pathogenesis of PAH. We first examined the activity of NF-κB in patients with PAH. We then used a rat model of monocrotaline (MCT)-induced PAH to examine whether NP-mediated delivery of the NF-κB decoy can attenuate the development of PAH.

Methods

Histopathologic and Immunohistochemical Examination of Human Lungs

Human lung tissue was obtained from autopsy specimens from 4 patients whose deaths were attributed to idiopathic PAH and 2

Received August 10, 2008; first decision August 26, 2008; revision accepted March 2, 2009.

From the Departments of Surgery (S.K., R.T.), Cardiovascular Medicine (K.E., L.C., K.N., E.I., M.M., K. Sunagawa), and Pathology (K. Sueishi), Graduate School of Medical Science, Kyushu University, Fukuoka; Hosokawa Powder Technology Research Institute (H.T., K.H.), Osaka; and Division of Clinical Gene Therapy (R.M.), Osaka University Medical School, Osaka, Japan.

Correspondence to Kensuke Egashira, Department of Cardiovascular Medicine, Graduate School of Medical Science, Kyushu University, 3-1-1, Maidashi, Higashi-ku, Fukuoka 812-8582, Japan. E-mail egashira@cardiol.med.kyushu-u.ac

Hypertension is available at http://hyper.ahajournals.org DOI: 10.1161/HYPERTENSIONAHA.108.121418

patients whose deaths were attributed to nonlung disease (Figure S1, available in the online data supplement at http://hyper.ahajournals.org). Additional details are provided in the online data supplement.

Preparation of NPs

The NF-κB decoy oligodeoxynucleotides labeled with or without fluorescein-isothiocyanate (FITC) were prepared as described previously.[10,11] The decoy is directed against the NF-κB binding site in the promoter region that corresponds with NF-κB–responsive genes and works to inhibit binding of this transcription factor to the promoter region.[10,11] PEG-PLGA NPs encapsulated with FITC, NF-κB decoy, or FITC-labeled NF-κB decoy were prepared using an emulsion solvent diffusion method.[13,14] The average diameter of PEG-PLGA NPs was 44 nm. To measure FITC release kinetics, FITC-NP was immersed in Tris-EDTA buffer, and the released FITC was measured. Additional details are provided in the online data supplement.

In Vivo Experiments With a Rat Model of MCT-Induced PAH

Rats were SC injected with 60 mg/kg of MCT, which induces severe PAH within 3 weeks.[5,16,17] In the prevention protocol, animals were assigned to either an untreated control group or a group that received a single intratracheal instillation of NF-κB decoy alone (50 μg), FITC-NP (1000 μg of PEG-PLGA), or NF-κB decoy NPs (50 μg of NF-κB decoy per 1000 μg of PEG-PLGA) immediately after MCT (n=6 each). For intratracheal instillation, a volume of 0.1 mL of phosphate buffer suspension of NP or NF-κB decoy was injected gently into the trachea of animals accompanied by an equal volume of air. The biodistribution of FITC in the lung was also examined 3, 7, and 14 days after intratracheal instillation of FITC only, FITC-NPs, or FITC-labeled NF-κB decoy NPs in rats injected with MCT. In the treatment protocol, rats were divided into 2 groups (rats treated with a single intratracheal instillation of phosphate buffer and rats treated with NF-κB decoy NPs; n=33 each) 21 days after MCT injection, when severe PAH had been established.

Hemodynamic Measurements

Three weeks after MCT administration, the animals were anesthetized with sodium pentobarbital, and then polyethylene catheters were inserted into the right ventricle (RV) through the jugular vein and the carotid artery for hemodynamic measurements. RV systolic pressure and systemic blood pressure were measured with a polygraph system (AP-601G, Nihon Kohden).[5]

Assessment of Right Heart Hypertrophy and Pulmonary Arterial Remodeling

After systemic arterial and RV pressure had been recorded, the animals were euthanized, and the lungs and heart were isolated. The RV wall was dissected from the left ventricle (LV) and ventricular septum (S). The wet weight of the RV and LV+S was determined, and RV hypertrophy was expressed as follows: RV/(LV+S).[5]

The lungs were perfused with a solution of 10% phosphate buffered formalin (pH 7.4). At the same time, 10% phosphate buffered formalin (pH 7.4) was administered into the lungs via the tracheal tube at a pressure of 20 cm H_2O. These specimens were processed for light microscopy by routine paraffin embedding. The degree of remodeling (muscularization) of the small peripheral pulmonary arteries was assessed by double immunohistochemical staining of the 3-μm sections with an anti–α-smooth muscle actin antibody (dilution 1:500, clone 1A4, Dako) and anti–platelet endothelial cell adhesion molecule 1 (M-20) antibody (dilution 1:100, Santa Cruz Biotechnology) modified from a protocol described elsewhere.[18]

To assess the type of remodeling in the muscular pulmonary arteries, microscopic images were analyzed. In each rat, 30 to 40 intra-acinar arteries were categorized as muscular (ie, with a complete medial coat of muscle), partially muscular (ie, with only a crescent of muscle), or nonmuscular (ie, with no apparent muscle). The arteries were counted and averaged within a range of diameters from 25 to 50 μm.

Histopathologic and Immunohistochemical Analysis

The degrees of monocyte infiltration were evaluated by immunostaining with the ED-1 (analogue of human CD68) antibody against monocytes. For quantification, a blind observer counted the number of ED-1–positive cells in 10 fields.[4] Monocytes were also subjected to immunostaining with antibodies against FITC, an epitope (α-p65) on the p65 subunit of NF-κB, or nonimmune mouse IgG. The α-p65 monoclonal antibody recognizes an epitope on the p65 subunit that is masked by bound inhibitor of κB (I-κB).[9] Therefore, this antibody exclusively detects activated NF-κB.[12]

Electrophoretic Mobility-Shift Assays

Nuclear extracts were prepared from the whole-lung homogenates using a nuclear extract kit (NE-PER Nuclear and Cytoplasmic Extraction Reagents, Thermo Science) according to the manufacturer's instructions. The protein was measured using a BCA Protein Assay kit (Thermo Science). For NF-κB activation, a nonradioactive electrophoresis mobility-shift assay kit (AY1030, Panomics) was used according to the manufacturer's instructions. Five μg of nuclear protein were incubated for 30 minutes at room temperature with a biotinylated oligonucleotide containing the NF-κB binding site, and then the samples were separated on a nondenaturing polyacrylamide gel and blotted onto a positively charged nylon membrane. After blotting, the oligos on the membrane were fixed using a UV cross-linker oven. Then, the membrane was incubated with streptavidin-horseradish-peroxidase solution at room temperature for 15 minutes and with detection reagents for 5 minutes. Nuclear proteins that were bound to the NF-κB binding site were detected by chemiluminescence with the use of the LAS-1000 detection system (Fujifilm).

Real-Time Quantitative RT-PCR

Real-time PCR amplification was performed with the rat cDNA with the use of the ABI PRI8:21 PM 7000 Sequence Detection System (Applied Biosystems), as described previously.[12] TaqMan primer/probes for MCP-1, TNF-α, IL-1, IL-6, intercellular adhesion molecule 1, and GAPDH, which served as the endogenous reference, were purchased from Applied Biosystems (Assay-on-Demand gene expression products Rn00580555, Rn99999017, Rn00580432, Rn00561420, and Rn00564227 and TaqMan Rodent GAPDH Control Reagents, respectively).

Intracellular Delivery of NPs Incorporated With an FITC-Labeled NF-κB Decoy to Human Monocytes and Pulmonary Arterial Smooth Muscle Cells

The human monocyte cell line THP-1 was obtained from the German Collection of Micro-organisms and Cell Cultures and was used between passages 4 and 8. Cells were cultured in RPMI 1640 with 10% FBS in a humidified atmosphere of 5% CO_2 in air. The cell density was adjusted to 10^6 cells per milliliter in 1 mL of serum-free medium in 35-mm-diameter dishes. The cells were serum deprived 24 hours before the experiment. The growth medium was replaced with FITC-conjugated NF-κB decoy encapsulated PEG-PLGA NP suspension medium (0.5 mg/mL) and then further incubated for 1 hour. At the end of the experiment, the cells were washed 3 times with PBS to eliminate excess NPs that were not incorporated into the cells. Then, the cells were fixed with 10% cold methanol, and nuclei were counterstained with propidium iodide. Cellular uptake of FITC-conjugated NF-κB decoy-encapsulated PEG-PLGA NPs was evaluated by fluorescence microscopy.

Human pulmonary artery smooth muscle cells (PASMCs) were obtained from Cambrex Bio Science, Inc, and cultured as described previously. Cells were used between passages 4 and 8. Human PASMCs were seeded on chambered cover glasses and incubated at 37°C/5% CO_2 until the cells were subconfluent. The following treatments were performed in the same manner.

Lipopolysaccharide-Induced Activation of Human Monocytes

Bacterial lipopolysaccharide (serotype 0111:B4; Sigma) was added at 1 μg/mL to the cells as indicated for each experiment. NF-κB decoy at 5 μg/mL, NF-κB decoy-encapsulated NPs containing 0.1 mg/mL of PEG-PLGA NP and 5 μg/mL of NF-κB decoy, or the vehicle alone was added to the wells simultaneously. Four hours later, the cells were washed 3 times with PBS. NF-κB pathway activity was measured using a TransAM NF-κB p65 ELISA-based assay kit (Active Motif). Nuclear extracts of THP-1 were prepared with the NE-PER kit (Pierce) according to the manufacturer's protocol. All of the procedures were carried out at 4°C. Protein concentration was determined by BCA assay, and 20 μg of protein from each sample were used in the assay. Samples were placed along with 30 μL of binding buffer on a 96-well plate to which oligonucleotides containing an NF-κB consensus binding site had been immobilized. Plates were incubated for 1 hour on a shaker. During this time, the activated NF-κB contained in the sample specifically bound to this nucleotide. The plate was then washed, and the NF-κB complex bound to the oligonucleotides was detected using a primary antibody (100 μL diluted 1:1000 in antibody binding buffer for 1 hour) that is directed against the NF-κB p65 subunit. The plate was then washed again, 100 μL of secondary antibody (diluted 1:1000 in antibody binding buffer) conjugated to horseradish peroxidase was added, and the plate was incubated for 1 hour. The plate was washed again, and 100 μL of developing solution were added. The plate was incubated for 4 minutes away from direct light, 100 μL of stop solution were added, and the plate was read using a plate reader at 450 nm.

Human PASMC Proliferation Assay

Human PASMCs were seeded on 96-well culture plates at 1×10^4 cells per well (n=6 per group) in smooth muscle cells–basal medium with 10% FBS. After 24 hours, the cells were starved for 48 hours in serum-free medium to obtain quiescent nondividing cells. After starvation, 10% FBS was added. Also, a concentration of 1 mg/mL of NF-κB decoy only, NF-κB decoy-encapsulated PEG-PLGA NPs (0.05 mg/mL of PEG-PLGA and 1 mg/mL of decoy), or FITC-encapsulated PEG-PLGA NPs was added to each well. Cells were incubated for another 24 hours after addition of 5′-bromo-2′-deoxyuridine. 5′-Bromo-2′-deoxyuridine incorporation was evaluated by an ELISA kit from Calbiochem.

Statistical Analysis

All of the results are expressed as the mean±SEM. Statistical analysis of differences was performed by ANOVA followed by Bonferroni's multiple comparison test. The survival rates were determined by the Kaplan–Meier method. $P<0.05$ was considered statistically significant.

Results

Activation of NF-κB Expression in Patients With PA6H and in MCT-Induced PAH Rats

Localization of NF-κB activation was examined by immunohistochemical studies in lung tissue from patients using the antibody against α-p65.[9] An intense immunoreactivity of α-p65 was noted primarily in alveolar macrophages and to some extent in small pulmonary arterial lesions (mainly in smooth muscle cells in the medium) from 4 patients with PAH (Figure 1A and Figure S1A). This NF-κB activation was associated with positive staining of MCP-1 and IL-6. In contrast, none at all of α-p65 was detected in 2 control patients whose deaths were not attributed to lung disease (Figure S1B).

In MCT-induced PAH rats, activation NF-κB was noted mainly in alveolar macrophages and weakly in pulmonary artery lesions 7 days after MCT administration (Figure 1B and 1C). An electrophoretic mobility-shift assay was performed to detect the DNA binding activity of NF-κB (Figure S2). The binding activity of the lung increased in rats after MCT injection, which peaked on day 3 and decreased on day 7.

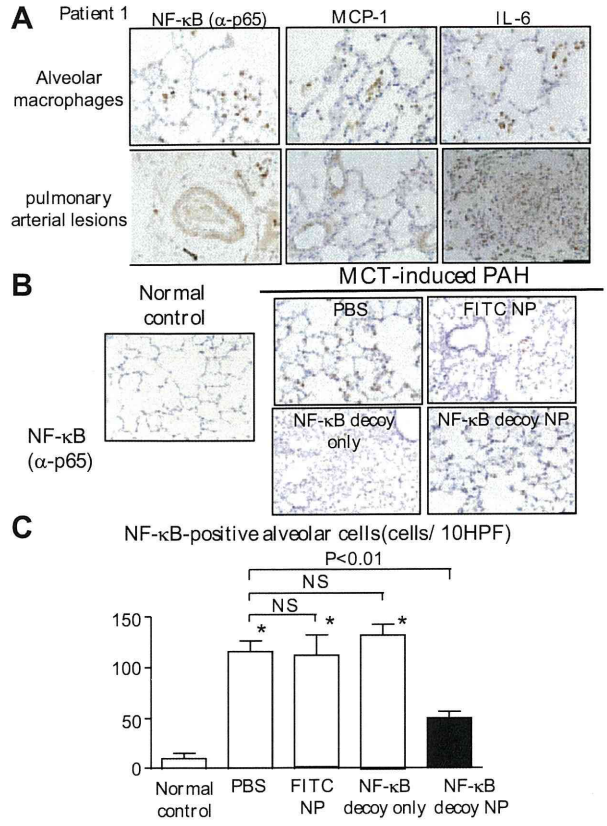

Figure 1. NF-κB activation in patients with PAH and rats with MCT-induced PAH and the effect of intratracheal instillation of NF-κB decoy NPs on NF-κB activation in rats. A, Micrographs of cross sections of the lung from patient 1 stained immunohistochemically with NF-κB (α-p65), MCP-1, and IL-6. Pictures stained with nonimmune IgG control are shown in the inset. Scale bar: 50 μm. B, Micrographs of cross sections of the lung stained immunohistochemically with NF-κB (α-p65) from normal rats and PAH rats 7 days after MCT injection. Scale bar: 50 μm. C, Effects of NF-κB decoy NPs on infiltration of NF-κB (α-p65)–positive cells 7 days after MCT injection. Data are mean±SEM (n=4 each). *$P<0.01$ vs PBS vs normal control.

Effects of Intratracheal Treatment With NF-κB Decoy NP on NF-κB Activation

Single intratracheal instillation of NF-κB decoy NPs, but not FITC NPs or NF-κB decoy only, resulted in marked attenuation of the increased NF-κB (α-p65) activity 7 days after MCT injection (Figure 1B and 1C). Treatment with NF-κB decoy NP markedly attenuated the DNA binding activity of NF-κB after MCT injection (Figure S2).

Because NF-κB was activated in alveolar monocytes and small pulmonary arterial smooth muscle cells in animals and humans with PAH, the effects of NF-κB decoy NPs on NF-κB activity were examined in the human monocyte cell line (THP-1) and in PASMCs in vitro (Figure S3). When those cultured cells were incubated with FITC-labeled NF-κB

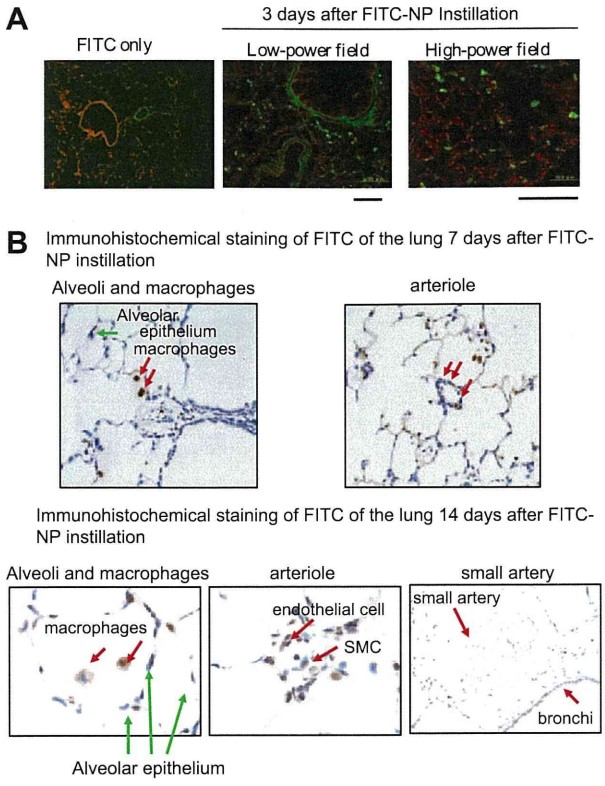

Figure 2. Localization of FITC after FITC-labeled NF-κB decoy NPs postinstillation in the rat lung. A, Fluorescent micrographs of cross sections from lung instillated with FITC only and FITC-labeled NF-κB decoy NPs on day 3 postinstillation. Nuclei were counterstained with propidium iodide (red). Scale bars: 100 μm. B, Micrographs of cross sections stained immunohistochemically against FITC from lung instillated intratracheally with FITC-NPs on days 7 and 14 postinstillation. Scale bars: 100 μm.

decoy NPs for 60 minutes, they were exclusively positive for intracellular localization of FITC. Treatment with NF-κB decoy NPs, but not but with FITC-NPs only or NF-κB decoy only, prevented NF-κB activation in THP-1 cells and attenuated proliferation of human PASMCs.

Localization of FITC-Labeled NF-κB Decoy NPs in the Lung of MCT-Induced PAH

Localization of FITC was examined after a single intratracheal instillation of FITC-labeled NF-κB decoy NPs in animals injected with MCT. Histopathologic examination of lung sections showed that strong FITC signals were detected only in FITC-NP–instillated lung 3 days after instillation, whereas no FITC signals were observed in control noninjected lungs or in lungs injected with FITC only (Figure 2A). There were the FITC-positive cells in bronchi and alveoli, alveolar macrophages, and small arteries. Immunofluorescent staining revealed FITC signals localized mainly in small arteries and arterioles, as well as in small bronchi and alveoli, 7 and 14 days after instillation of FITC-NPs (Figure 2B). FITC signals were not detected in remote organs (liver, spleen, kidney, and heart) on days 1, 3, and 7 (data not shown).

Effects of NF-κB Decoy NP on the Development of PAH in the Rat Model of MCT-Induced PAH

As reported previously by us and by other investigators,[5,16,17] the injection of MCT results in severe PAH (increased RV systolic pressure and RV hypertrophy; Figure 3) associated with small pulmonary arterial remodeling (Figure 4) and increased infiltration of ED-1–positive monocytes (Figure 4) 3 weeks after MCT injection. Single intratracheal treatment with NF-κB decoy NPs but not with NF-κB decoy only or FITC-NPs attenuated the development of PAH (Figure 3), small pulmonary arterial remodeling (Figure 4), and inflammation (Figure 4).

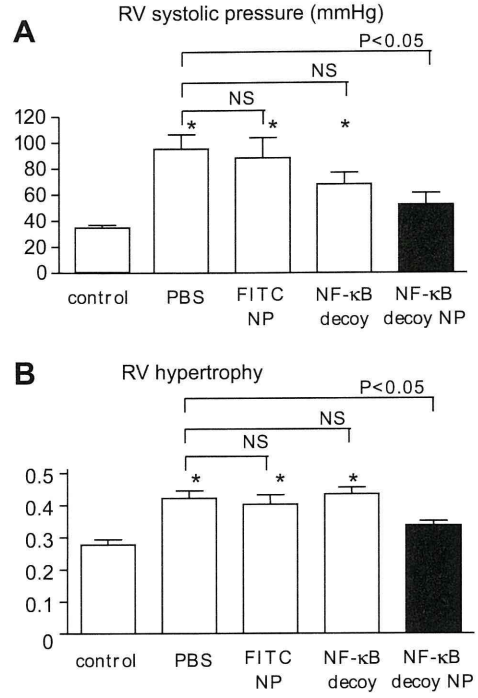

Figure 3. Effects of NF-κB decoy NPs on RV systolic pressure and RV hypertrophy 3 weeks after MCT injection. A, RV systolic pressure 21 days after MCT injection in 4 groups. Data are mean±SEM (n=6 each). *$P<0.05$ vs normal control. B, RV hypertrophy (the ratio of RV/[LV+S]) 21 days after MCT injection in the different treatment groups. Data are mean±SEM (n=6 each). *$P<0.05$ vs normal control.

Effects of NF-κB Decoy NPs on Expression of Proinflammatory Factors

As reported previously,[3,4] MCT-induced PAH was associated with increased gene expression of proinflammatory factors. Treatment with NF-κB decoy NPs significantly reduced the increased gene expression of MCP-1, TNF-α, and IL-1β (Figure 5). NF-κB decoy NPs tended to decrease the expression of IL-6 and intercellular adhesion molecule-1.

In Vitro NP Release Kinetics

An analysis of the in vitro FITC release kinetics from FITC-NP showed an early burst of FITC release such that ≈40% of the total amount ultimately released was present on day 1, followed by sustained release of the remaining FITC over the next 28 days (Figure S4).

Effects of NF-κB Decoy NPs on Survival

Treatment with NF-κB decoy NPs 21 days after MCT injection significantly ($P<0.01$) improved the survival rate (Figure 6).

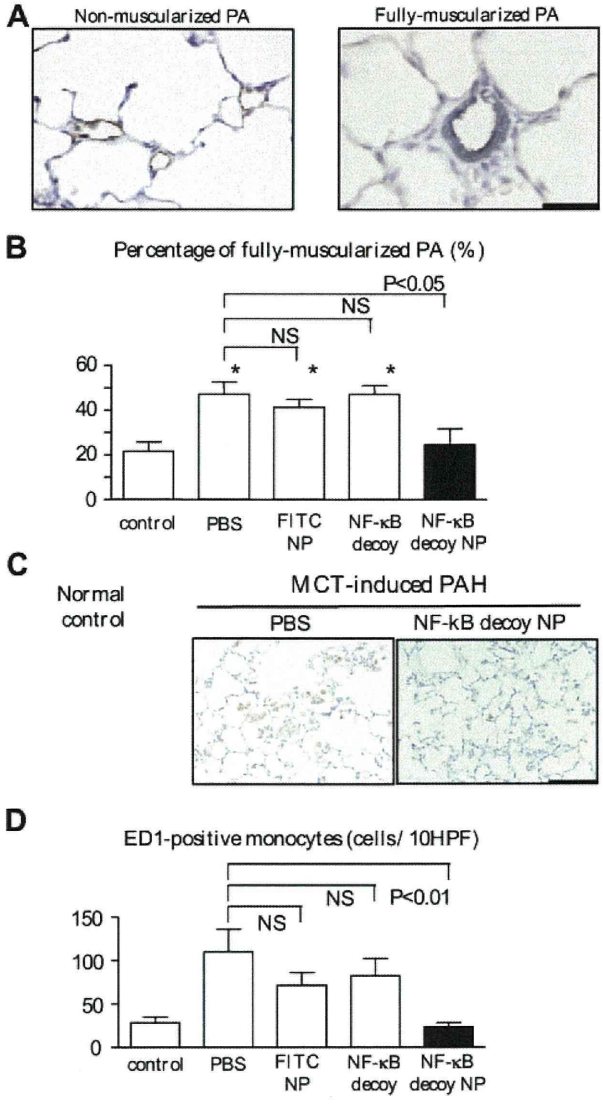

Figure 4. Effects of NF-κB decoy NPs on small pulmonary arterial remodeling and infiltration of monocytes. A, Representative micrographs of nonmuscularized and fully muscularized small pulmonary arteries stained immunohistochemically against the endothelial layer (brown) and medial smooth muscle cells (blue). Scale bar: 50 μm. B, The percentage of fully muscularized small pulmonary arteries in the different treatment groups. Data are mean±SEM (n=6 each). *$P<0.05$ vs normal control. C, Representative micrographs of pulmonary alveoli stained immunohistochemically for ED-1–positive monocytes. Scale bar: 50 μm. D, Infiltration of ED-1–positive monocytes into the lung (the number of positive cells per 10 high-power field cross sections). Data are mean±SEM (n=6 each). *$P<0.01$ vs normal control.

Discussion

The present study demonstrates for the first time that intratracheal instillation of PEG-PLGA NPs is an excellent system for drug delivery of NF-κB decoy to the lung. The FITC signals were detected not only in small bronchial tracts but also in alveolar macrophages and small pulmonary arteries for ≤14 days after a single instillation. After cellular uptake of NPs, NPs might slowly release encapsulated decoy into the cytoplasm as PLGA is hydrolyzed. This might protect the encapsulated decoy from intracellular degradation before its arrival at the nuclear target. Our in vitro studies in cultured human monocytes and pulmonary arterial smooth muscle cells support this notion. Therefore, this platform nanotechnology may represent a novel NP-mediated drug delivery system for treatment of severe lung diseases, including PAH.

The present study also reports a pivotal role of NF-κB in the pathogenesis of PAH. Recently, Sawada et al[19] and Huang et al[20] reported that systemic daily administration of pyrrolidine dithiocarbamate, a nonspecific inhibitor of NF-κB, attenuated the development of MCT-induced PAH. Pyrrolidine dithiocarbamate is known to be a low molecular weight thiol compound and has anti-inflammatory and antioxidant activity independent of the NF-κB pathway. Indeed, in a study by Huang et al,[20] pyrrolidine dithiocarbamate treatment had no effect on MCT-induced NF-κB activation. In contrast, we found in the present study that NF-κB is activated in alveolar macrophages and small pulmonary arteries associated with NF-κB–dependent inflammatory factors (eg, MCP-1, IL-1, and TNF-α) in patients with PAH and rats with MCT-induced PAH, and blockade of NF-κB activation by a single intratracheal instillation of NF-κB decoy NPs reduced inflammatory changes. These data suggest that NF-κB might be pivotal in mediating inflammatory changes seen in PAH.

We also found that intratracheal instillation of NF-κB decoy NPs prevented the development of PAH (increased RV pressure, RV hypertrophy, and pulmonary artery remodeling) in the prevention protocol. We and others have reported that blockade of MCP-1 reduces vascular pathology after vascular injury[9,21–25] and the development of PAH.[5,6] In addition, as we reported in human coronary artery smooth muscle cells in vitro,[12,26] we found that NF-κB decoy NPs attenuated proliferation of human PASMCs in vitro. Therefore, the beneficial effects of NF-κB decoy NPs can be attributable to inhibition of inflammation and smooth muscle cell proliferation resulting from reduced NF-κB activation.

Furthermore, we found that a single intratracheal treatment of NF-κB decoy NPs 3 weeks after MCT injection improved survival rate in the treatment protocol, suggesting that this NP-mediated NF-κB decoy delivery may have significant therapeutic effects. We did not examine the therapeutic effects of repetitive intratracheal instillation of NF-κB decoy NPs, because it is technically difficult to perform multiple intratracheal instillation of this NP system in rats and other small animals. For translation of our present findings into clinical medicine, further studies are needed to investigate whether repetitive delivery of NPs into lungs produces greater therapeutic effects over time.

Several points are worth mentioning with regard to potential clinical applicability. First, from a toxicological point of view, no adverse reactions, eg, pulmonary inflammation, after exposure to a single intratracheal instillation of FITC-NPs (PEG-PLGA at 1 mg per body) or NF-κB decoy NPs (NF-κB decoy at 50 μg per body in rats weighing 250 to 300 g) were noted in the rat model, suggesting that the NPs used in this study may not cause an adverse reaction. However, the 3-week observation period for this NP system might be too short to determine its safety. Second, we reported recently that neither intravenous injection of the NF-κB decoy at 1 mg per body in monkeys nor deployment

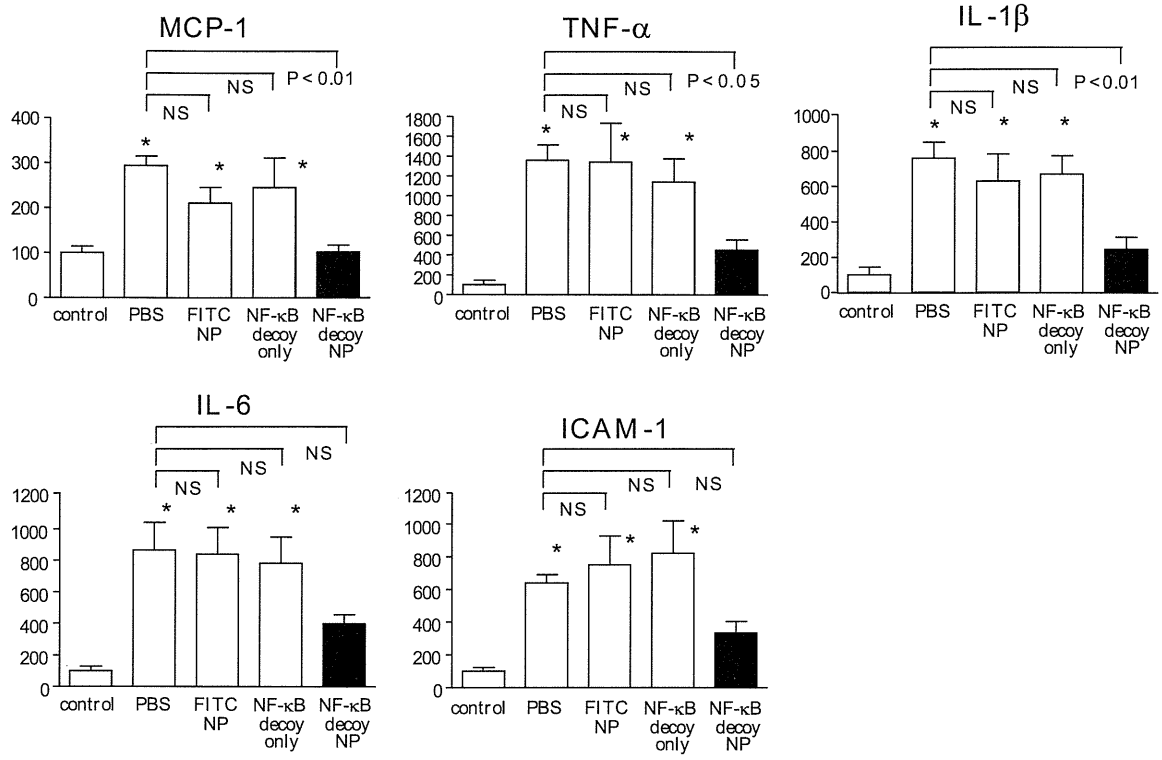

Figure 5. Effects of NF-κB decoy NPs on mRNA levels of various inflammatory and proliferative factors 21 days after MCT injection (n=5 each). *$P<0.01$ vs normal control.

of an NF-κB decoy-eluting stent (≈600 μg per stent) in rabbits showed systemic adverse effects.[12] More important are the findings of a clinical trial that we completed recently to test the feasibility and safety of the NF-κB decoy. The decoy was transfected into the stented coronary artery sites at doses of 1000, 2000, or 4000 μg per body via a channel balloon catheter immediately after successful percutaneous coronary intervention in 18 patients with flow-limiting coronary stenosis.[27] The patients showed low restenosis rates and no evidence of systemic adverse effects during the 6-month observation period. These data support the notion that NF-κB decoy can be applied in a clinical setting. Third, this NP system itself is not suitable for inhalant therapy, because it is known that most inhaled NPs are exhaled rather than being delivered into the lung.[28] In contrast, microparticles with aerodynamic diameters between 2 and 8 μm reach small bronchi. However, the microparticles are easily recognized and eliminated by the mucociliary clearance system and alveolar macrophages immediately after they reach the small bronchi.[28] In contrast, polymeric NPs escape the clearance system of the lung when they are delivered into small bronchi and are, thus, taken up by alveoli, macrophages, and pulmonary small vessels. Therefore, to use this NP system for inhalant therapy, we need to develop the nanocomposite microsized particles[28] that will decompose to NPs after reaching the small bronchi.

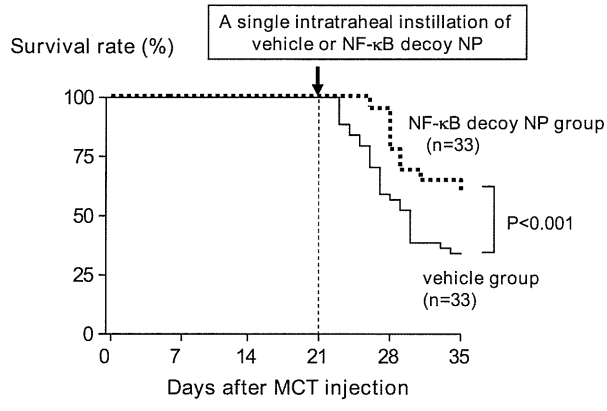

Figure 6. Effects of NF-κB decoy NPs on survival rate. Survival rate analyzed by the Kaplan–Meier method in vehicle and NF-κB decoy NP groups.

Perspectives

This study has shown that NF-κB is activated in pulmonary arterial lesions in patients with PAH and in rats with MCT-induced PAH, and blockade of NF-κB by NP-mediated NF-κB decoy delivery not only prevented the development of MCT-induced PAH in the prevention protocol but also improved survival rate in the treatment protocol. These data support the notion that NF-κB plays a pivotal role in the pathogenesis of PAH and, thus, represents a new therapeutic target for PAH. This nanotechnology platform may be developed as a more effective and less invasive nanomedicine in PAH therapy.

Sources of Funding

This study was supported by Grants-in-Aid for Scientific Research (19390216 and 19650134) from the Ministry of Education, Science, and Culture (Tokyo, Japan) and by Health Science Research grants

(Research on Translational Research and Nano-medicine) from the Ministry of Health, Labor, and Welfare (Tokyo, Japan).

Disclosures

K.E. and R.M. hold a patent on the results reported in this study. The remaining authors report no conflicts.

References

1. Farber HW, Loscalzo J. Pulmonary arterial hypertension. *N Engl J Med.* 2004;351:1655–1665.
2. Humbert M, Sitbon O, Simonneau G. Treatment of pulmonary arterial hypertension. *N Engl J Med.* 2004;351:1425–1436.
3. Stenmark KR, Fagan KA, Frid MG. Hypoxia-induced pulmonary vascular remodeling: cellular and molecular mechanisms. *Circ Res.* 2006; 99:675–691.
4. Sanchez O, Marcos E, Perros F, Fadel E, Tu L, Humbert M, Dartevelle P, Simonneau G, Adnot S, Eddahibi S. Role of endothelium-derived CC chemokine ligand 2 in idiopathic pulmonary arterial hypertension. *Am J Respir Crit Care Med.* 2007;176:1041–1047.
5. Ikeda Y, Yonemitsu Y, Kataoka C, Kitamoto S, Yamaoka T, Nishida K, Takeshita A, Egashira K, Sueishi K. Anti-monocyte chemoattractant protein-1 gene therapy attenuates pulmonary hypertension in rats. *Am J Physiol Heart Circ Physiol.* 2002;283:H2021–H2028.
6. Kimura H, Kasahara Y, Kurosu K, Sugito K, Takiguchi Y, Terai M, Mikata A, Natsume M, Mukaida N, Matsushima K, Kuriyama T. Alleviation of monocrotaline-induced pulmonary hypertension by antibodies to monocyte chemotactic and activating factor/monocyte chemoattractant protein-1. *Lab Invest.* 1998;78:571–581.
7. Katsushi H, Kazufumi N, Hideki F, Katsumasa M, Hiroshi M, Kengo K, Hiroshi D, Nobuyoshi S, Tetsuro E, Hiromi M, Tohru O. Epoprostenol therapy decreases elevated circulating levels of monocyte chemoattractant protein-1 in patients with primary pulmonary hypertension. *Circ J.* 2004;68:227–231.
8. Itoh T, Nagaya N, Ishibashi-Ueda H, Kyotani S, Oya H, Sakamaki F, Kimura H, Nakanishi N. Increased plasma monocyte chemoattractant protein-1 level in idiopathic pulmonary arterial hypertension. *Respirology.* 2006;11:158–163.
9. Brand K, Page S, Rogler G, Bartsch A, Brandl R, Knuechel R, Page M, Kaltschmidt C, Baeuerle PA, Neumeier D. Activated transcription factor nuclear factor-kappa B is present in the atherosclerotic lesion. *J Clin Invest.* 1996;97:1715–1722.
10. Morishita R, Higaki J, Tomita N, Ogihara T. Application of transcription factor "decoy" strategy as means of gene therapy and study of gene expression in cardiovascular disease. *Circ Res.* 1998;82:1023–1028.
11. Kitamoto S, Egashira K, Kataoka C, Koyanagi M, Katoh M, Shimokawa H, Morishita R, Kaneda Y, Sueishi K, Takeshita A. Increased activity of nuclear factor-kappaB participates in cardiovascular remodeling induced by chronic inhibition of nitric oxide synthesis in rats. *Circulation.* 2000; 102:806–812.
12. Ohtani K, Egashira K, Nakano K, Zhao G, Funakoshi K, Ihara Y, Kimura S, Tominaga R, Morishita R, Sunagawa K. Stent-based local delivery of nuclear factor-kappaB decoy attenuates in-stent restenosis in hypercholesterolemic rabbits. *Circulation.* 2006;114:2773–2779.
13. Murakami H, Kobayashi M, Takeuchi H, Kawashima Y. Preparation of poly(DL-lactide-co-glycolide) nanoparticles by modified spontaneous emulsification solvent diffusion method. *Int J Pharm.* 1999;187:143–152.
14. Kawashima Y, Yamamoto H, Takeuchi H, Hino T, Niwa T. Properties of a peptide containing DL-lactide/glycolide copolymer nanospheres prepared by novel emulsion solvent diffusion methods. *Eur J Pharm Biopharm.* 1998;45:41–48.
15. Panyam J, Zhou WZ, Prabha S, Sahoo SK, Labhasetwar V. Rapid endo-lysosomal escape of poly(DL-lactide-co-glycolide) nanoparticles: implications for drug and gene delivery. *FASEB J.* 2002;16:1217–1226.
16. Schermuly RT, Dony E, Ghofrani HA, Pullamsetti S, Savai R, Roth M, Sydykov A, Lai YJ, Weissmann N, Seeger W, Grimminger F. Reversal of experimental pulmonary hypertension by PDGF inhibition. *J Clin Invest.* 2005;115:2811–2821.
17. Cowan KN, Heilbut A, Humpl T, Lam C, Ito S, Rabinovitch M. Complete reversal of fatal pulmonary hypertension in rats by a serine elastase inhibitor. *Nat Med.* 2000;6:698–702.
18. Quinlan TR, Li D, Laubach VE, Shesely EG, Zhou N, Johns RA. eNOS-deficient mice show reduced pulmonary vascular proliferation and remodeling to chronic hypoxia. *Am J Physiol Lung Cell Mol Physiol.* 2000;279:L641–L650.
19. Sawada H, Mitani Y, Maruyama J, Jiang BH, Ikeyama Y, Dida FA, Yamamoto H, Imanaka-Yoshida K, Shimpo H, Mizoguchi A, Maruyama K, Komada Y. A nuclear factor-kappaB inhibitor pyrrolidine dithiocarbamate ameliorates pulmonary hypertension in rats. *Chest.* 2007;132: 1265–1274.
20. Huang J, Kaminski PM, Edwards JG, Yeh A, Wolin MS, Frishman WH, Gewitz MH, Mathew R. Pyrrolidine dithiocarbamate restores endothelial cell membrane integrity and attenuates monocrotaline-induced pulmonary artery hypertension. *Am J Physiol Lung Cell Mol Physiol.* 2008;294: L1250–L1259.
21. Egashira K. Molecular mechanisms mediating inflammation in vascular disease: special reference to monocyte chemoattractant protein-1. *Hypertension.* 2003;41:834–841.
22. Egashira K. Clinical importance of endothelial function in arteriosclerosis and ischemic heart disease. *Circ J.* 2002;66:529–533.
23. Ohtani K, Usui M, Nakano K, Kohjimoto Y, Kitajima S, Hirouchi Y, Li XH, Kitamoto S, Takeshita A, Egashira K. Antimonocyte chemoattractant protein-1 gene therapy reduces experimental in-stent restenosis in hypercholesterolemic rabbits and monkeys. *Gene Ther.* 2004;11: 1273–1282.
24. Usui M, Egashira K, Ohtani K, Kataoka C, Ishibashi M, Hiasa K, Katoh M, Zhao Q, Kitamoto S, Takeshita A. Anti-monocyte chemoattractant protein-1 gene therapy inhibits restenotic changes (neointimal hyperplasia) after balloon injury in rats and monkeys. *FASEB J.* 2002;16: 1838–1840.
25. Egashira K, Zhao Q, Kataoka C, Ohtani K, Usui M, Charo IF, Nishida K, Inoue S, Katoh M, Ichiki T, Takeshita A. Importance of monocyte chemoattractant protein-1 pathway in neointimal hyperplasia after periarterial injury in mice and monkeys. *Circ Res.* 2002;90:1167–1172.
26. Lemarie CA, Esposito B, Tedgui A, Lehoux S. Pressure-induced vascular activation of nuclear factor-kappaB: role in cell survival. *Circ Res.* 2003; 93:207–212.
27. Egashira K, Suzuki J, Ito H, Aoki M, Isobe M, Morishita R. Long-term follow up of initial clinical cases with NF-kappaB decoy oligodeoxynucleotide transfection at the site of coronary stenting. *J Gene Med.* 2008; 10:805–809.
28. Tomoda K, Ohkoshi T, Kawai Y, Nishiwaki M, Nakajima T, Makino K. Preparation and properties of inhalable nanocomposite particles: effects of the temperature at a spray-dryer inlet upon the properties of particles. *Colloids Surf B Biointerfaces.* 2008;61:138–144.

Circulation Research
JOURNAL OF THE AMERICAN HEART ASSOCIATION

American Heart Association®
Learn and Live℠

Acquisition of Brain Na Sensitivity Contributes to Salt-Induced Sympathoexcitation and Cardiac Dysfunction in Mice With Pressure Overload

Koji Ito, Yoshitaka Hirooka and Kenji Sunagawa

Circ. Res. 2009;104;1004-1011; originally published online Mar 19, 2009;
DOI: 10.1161/CIRCRESAHA.108.188995
Circulation Research is published by the American Heart Association. 7272 Greenville Avenue, Dallas, TX 72514
 Print ISSN: 0009-7330. Online ISSN: 1524-4571

Acquisition of Brain Na Sensitivity Contributes to Salt-Induced Sympathoexcitation and Cardiac Dysfunction in Mice With Pressure Overload

Koji Ito, Yoshitaka Hirooka, Kenji Sunagawa

Abstract—In animal models of salt-sensitive hypertension, high salt augments sympathetic outflow via central mechanisms. It is not known, however, whether pressure overload affects salt sensitivity, thereby modifying central sympathetic outflow and cardiac function. We induced left ventricular hypertrophy with aortic banding in mice. Four weeks after aortic banding (AB-4), the left ventricle wall thickness was increased without changing the percentage fractional shortening. AB-4 mice were then fed either a high-salt (8%) diet or regular-salt diet for additional 4 weeks. Cardiac dysfunction, wall thickness, and 24-hour urinary catecholamine excretion were increased with high-salt diet compared with regular-salt diet. We then examined brain Na sensitivity. Intracerebroventricular infusion of high-Na (0.2 mol/L) artificial cerebrospinal fluid into AB-4 mice and mice Sham-4 increased urinary catecholamine excretion, arterial pressure, and heart rate more in AB-4 mice than in Sham-4 mice. Intracerebroventricular infusion of an epithelial Na channel blocker (benzamil) into mice with high-salt diet significantly decreased urinary catecholamine excretion and improved cardiac function. Infusion of either an angiotensin II type 1 receptor blocker or a Rho-kinase inhibitor also attenuated the salt-induced sympathetic hyperactivation and cardiac dysfunction in mice with high-salt diet. The levels of angiotensin II type 1 receptor and phosphorylated moesin, a substrate of Rho-kinase, were significantly greater in AB-4 mice than in Sham-4 mice. These results suggest that mice with pressure overload acquire brain Na sensitivity because of the activation of epithelial Na channel via Rho-kinase and angiotensin II, and this mechanism contributes to salt-induced sympathetic hyperactivation, further pressure overload, and cardiac dysfunction. (***Circ Res.* 2009;104:1004-1011.**)

Key Words: hypertension ■ heart failure ■ hypertrophy ■ sympathetic nervous system ■ brain ■ sodium chloride

As an environmental factor, high salt intake increases sympathetic activity in genetic models of hypertension.[1–3] In these salt-sensitive hypertensive rats, central mechanisms, such as enhanced Na sensitivity, as well as renal mechanisms contribute to high salt–induced sympathetic activation and arterial pressure elevation.[1–3] Enhanced central sympathetic outflow is also observed in animal models of heart failure,[4–7] and intracerebroventricular (ICV) infusion of an amiloride analog, benzamil, which inhibits the epithelium Na^+ channels (ENaCs), may reduce the enhanced sympathetic drive and improve cardiac function in rats with myocardial infarction.[4]

The effects of sustained cardiac pressure overload on cardiac function and/or cardiac muscles have been investigated using aortic banding models.[8,9] It is not known whether the sustained cardiac pressure overload without a genetic predisposition to salt sensitivity influences brain Na sensitivity. Furthermore, few studies have examined the relationship between central sympathetic outflow and cardiac function in animals with pressure overload. Therefore, the aim of the present study was to determine whether a sustained pressure overload produced in mice without a genetic predisposition to salt sensitivity induces brain Na sensitivity, thereby enhancing the central sympathetic outflow leading to cardiac dysfunction. For this purpose, we examined the effects of high salt intake on brain Na concentration, sympathetic activity, arterial pressure, and cardiac function in mice with pressure overload produced by aortic banding. To elucidate brain Na sensitivity, we infused high-Na artificial cerebrospinal fluid (aCSF) ICV in mice with or without pressure overload induced by aortic banding and evaluated sympathetic activity and arterial pressure. In addition, to determine whether brain Na sensitivity is acquired in this model, we examined the effects of the ENaC blocker benzamil[4,5] on high salt–induced activation of the sympathetic nervous system and arterial pressure elevation, because ENaCs on the blood side of the choroidal epithelium may have an important role in Na transport into the CSF, as well as Na^+-K^+ ATPase on the CSF side of choroidal epithelium.[3,10,11] In addition, to explore the mechanisms involved, we also evaluated the role of brain

Original received October 7, 2008; revision received March 5, 2009; accepted March 10, 2009.

From the Department of Cardiovascular Medicine, Kyushu University Graduate School of Medical Sciences, Fukuoka, Japan.

Correspondence to Yoshitaka Hirooka, MD, PhD, FAHA, Department of Cardiovascular Medicine, Kyushu University Graduate School of Medical Sciences, 3-1-1, Higashi-ku, Fukuoka 812-8582, Japan. E-mail hyoshi@cardiol.med.kyushu-u.ac.jp

Circulation Research **is available at http://circres.ahajournals.org** **DOI: 10.1161/CIRCRESAHA.108.188995**

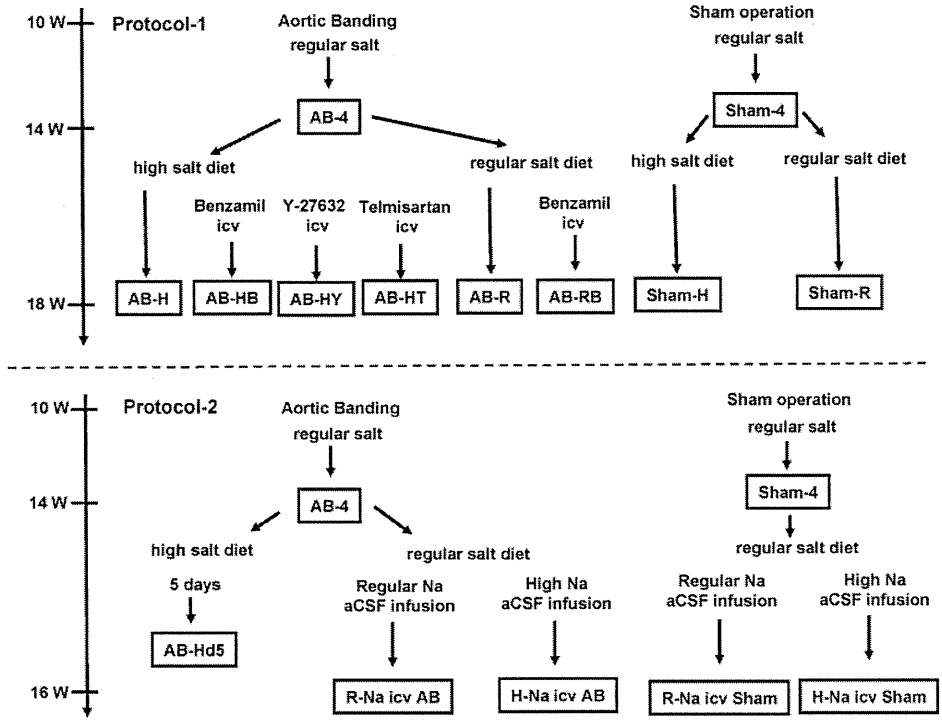

Figure 1. Experimental protocol and time line. W indicates weeks.

ENaCs in the enhanced sympathetic activity and cardiac dysfunction induced by high salt intake in mice with pressure overload and the relationship of brain ENaCs to the Rho/Rho-kinase pathway and the renin–angiotensin system (RAS) in the brain, because ENaCs in kidney are reported to be activated by the Rho/Rho-kinase pathway[12] and RAS.[13]

Materials and Methods

Animals

The study was reviewed and approved by the Committee on Ethics of Animal Experiments, Kyushu University Graduate School of Medical Sciences, and conducted according to the Guidelines for Animal Experiments of Kyushu University. Male Institute of Cancer Research (ICR) mice (10 weeks old; SLC, Fukuoka, Japan) were used.

Mouse Pressure Overload Model Preparation

The suprarenal abdominal aorta was banded in ICR mice (AB mice) to create the pressure overload model[14] or sham operation (Sham mice) as a control. We divided these mice into the groups represented in Figure 1. For details, see the online data supplement, available at http://circres.ahajournals.org.

Evaluation of Cardiac Function

Cardiac function was evaluated by echocardiography.[15,16] Serial M-mode echocardiography was performed under light sodium pentobarbital anesthesia with spontaneous respiration. Cardiac function was also evaluated by the left ventricular end-diastolic pressure (LVEDP). A conductance catheter (1.4 Fr; Miller Instruments) was inserted into the right carotid artery and advanced across the aortic valve into the left ventricle. See the online data supplement for details.

Measurement of Arterial Pressure and Heart Rate

Under sodium pentobarbital anesthesia and mechanical ventilation, a catheter was inserted into the right carotid artery and arterial pressure and heart rate were measured. In another protocol, we also measured arterial pressure and heart rate in awake AB mice fed a high-salt diet (AB-H) and AB mice fed with a regular salt diet (AB-R) using a radiotelemetry system implanted in the left carotid artery.[17] See the online data supplement for details.

Evaluation of Sympathetic Activity

Sympathetic activity was evaluated by measuring 24-hour urinary norepinephrine (U-NE) and urinary epinephrine (U-E) excretion using high-performance liquid chromatography.[15,18]

Evaluation of Na Sensitivity

We evaluated U-NE, U-E, arterial pressure, and heart rate responses to a high-salt diet or high-Na aCSF (0.2 mol/L, 1 μL/min for 10 minutes) ICV infusion in each group. In addition, we measured Na concentrations in the brain tissue (circumventricular tissues including the hypothalamus) of mice in each group. Furthermore, to examine the response of other central stimuli, we performed ICV infusion of angiotensin II (0.5 nmol/L, 1 μL/min for 5 minutes) and carbachol (0.1 mmol/L, 1 μL/min for 5 minutes). See the online data supplement for details.

Measurement of Organ Weight

After completion of the experiments, mice were killed with an overdose of sodium pentobarbital, and the heart and lungs were removed and weighed.

Measurement of Serum Parameters

We measured the serum concentrations of sodium, creatinine, and aldosterone in each group. See the online data supplement for details.

Evaluation of the Effects of Na Channel Blockade in the Brain

To assess the effects of Na channel blockade in the brain, benzamil, a specific ENaC blocker, was infused ICV (1 mg/ml, 0.11 μL/h for 28 days[14]). The U-NE and U-E excretion, arterial pressure, heart rate, and organ weight were measured, and echocardiography was per-

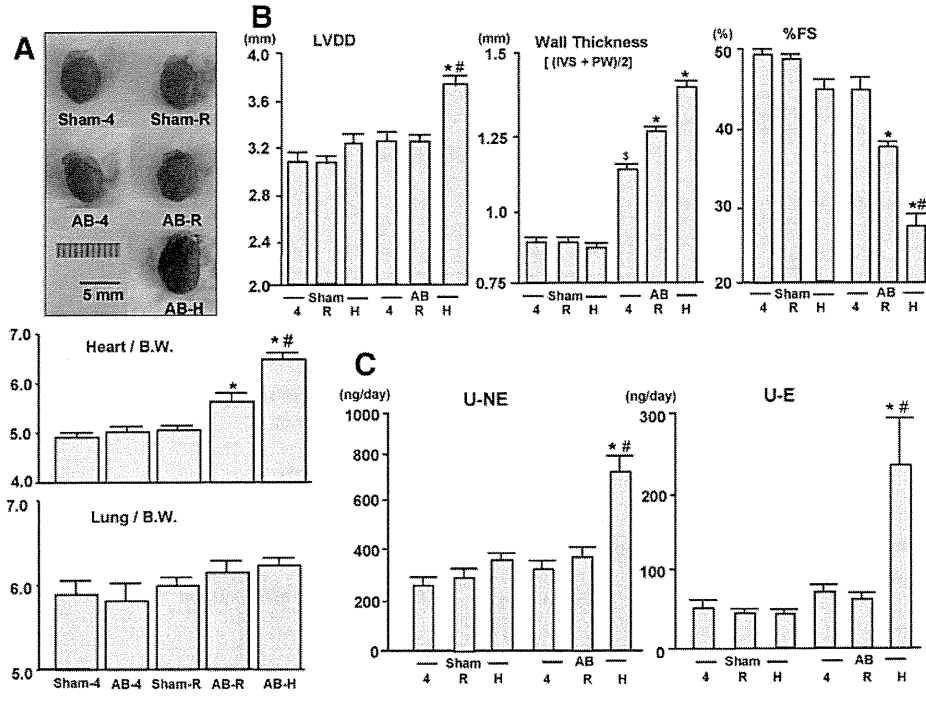

Figure 2. A, Example of the heart in each group and the relative heart and lung weight in each group. *$P<0.05$ vs Sham-4 and Sham-R, #$P<0.05$ vs AB-R (n=6 in each group). B, Cardiac function evaluation by echocardiography in each group. IVS, interventricular septum; PW, posterior wall. *$P<0.05$ vs Sham-R, #$P<0.05$ vs AB-R, \$$P<0.05$ vs Sham-4 (n=8 in each group). C, The 24-hour U-NE and U-E excretion in each group. *$P<0.05$ vs Sham-4 and Sham-R, #$P<0.05$ vs AB-R (n=10 in each group).

formed as described earlier. See the online data supplement for details.

Evaluation of the Effects of Rho-Kinase and Angiotensin Type 1 Receptor Blockade in the Brain

To assess the effects of Rho-kinase or angiotensin II type 1 receptor (AT_1R) blockade in the brain, Y-27632 (a specific Rho-kinase inhibitor[18]) or telmisartan (an AT_1R blocker) was infused ICV (Y-27632: 5 mmol/L, 0.11 μL/h for 28 days; telmisartan: 4 and 20 mmol /L, 0.11 μL/h for 28 days). The U-NE and U-E excretion, arterial pressure, heart rate, and organ weight were measured, and echocardiography was performed as described earlier. See the online data supplement for details.

Evaluation of AT_1R Expression and Rho-Kinase Activity

To assess AT_1R expression levels and Rho-kinase activity, we performed a Western blot analysis for AT_1R (1:1000, Santa Cruz Biotechnology, Santa Cruz, Calif) and phosphorylated-moesin, a substrate of Rho-kinase[19] (p-moesin, 1:1000, Santa Cruz Biotechnology) in the circumventricular tissues, including the hypothalamus and brain stem tissues, of Sham-4 mice and AB-4 mice. See the online data supplement for details.

Statistical Analysis

All values are expressed as means±SE. ANOVA was used to compare U-NE and U-E excretion, organ weight, left ventricular end-diastolic diameter (LVDD), left ventricular wall thickness (LVWT), percentage fractional shortening (%FS), and arterial pressure measured by telemetry between groups. An unpaired *t* test was used to compare changes in arterial pressure and heart rate after high-Na ICV infusion, as well as protein levels, between Sham mice and AB mice. Differences were considered to be significant when $P<0.05$.

Results

Characteristics of the Pressure Overload Model

Relative heart weight (heart weight/body weight) was not increased in AB-4 mice compared with Sham-4 mice (Figure 2A). AB-R mice, however, had a significantly higher relative heart weight than Sham-R mice and a significantly lower relative heart weight than AB-H mice. Relative lung weight (lung weight/body weight) did not differ between groups (Figure 2A). Body weight of AB mice was significantly lower than that of Sham mice (body weight: Sham-4, 44.7±1.4 g; AB-4, 45.3±1.1 g; Sham-R, 47.8±0.5 g; AB-R, 42.5±0.6 g; AB-H 40.6±0.9 g, n=6 for each); however, the absolute heart weight in AB-H was significantly greater than that in AB-R or Sham-R mice (heart weight: AB-H 0.26±0.01 g; Sham-R 0.24±0.01 g; AB-R 0.24±0.01 g; n=6 for each).

Echocardiography revealed the following characteristics: LVWT was greater in AB-4 mice than in Sham-4 mice, but %FS did not differ between the groups (Figure 2B). After an additional 4 weeks, cardiac function declined in AB-R mice compared with Sham-R mice and declined significantly more in AB-H mice compared with AB-R mice. LVDD was also higher in AB-H mice than in AB-R mice (Figure 2B).

Sympathetic activity was not significantly different among the AB-4 mice, AB-R mice, Sham-4 mice, and Sham-R mice. U-NE and U-E excretion was significantly higher, however, in AB-H mice compared with the other groups (Figure 2C).

LVEDP was significantly higher in AB-4 mice than in Sham-4 mice. In addition, LVEDP in AB-H mice further increased compared with Sham-R or AB-R mice (Table I in the online data supplement).

Arterial Pressure Monitoring

Measurement Under Anesthesia

Mean arterial pressure and heart rate were significantly higher in AB-4 mice compared with Sham-4 mice. In AB-R and AB-H mice, arterial pressure was reduced to levels similar to that in the Sham-R mice. Heart rate was significantly higher in AB-4, AB-R, and AB-H mice than in Sham-4

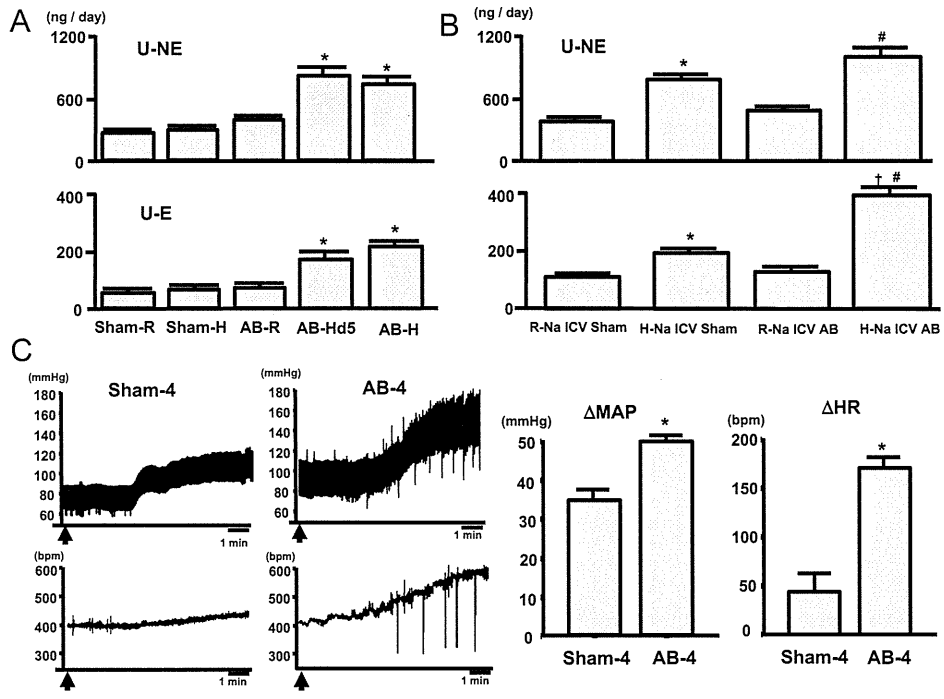

Figure 3. A, The 24-hour U-NE and U-E excretion in each group (response of sympathetic activity to high-salt diets). *$P<0.05$ vs Sham-R, Sham-H, and AB-R (n=10 in each group). B, The 24-hour U-NE and U-E excretion in each group (response of sympathetic activity to high-Na aCSF ICV infusion). *$P<0.05$ vs ICV R-Na Sham, #$P<0.05$ vs ICV R-Na AB, †$P<0.05$ vs high-Na ICV Sham (n=5 in each group). C, Response of arterial pressure and heart rate to ICV high-Na aCSF infusion. Left, Representative recordings from Sham-4 and AB-4 showing arterial pressure and heart rate response to ICV high-Na aCSF infusion. Right, Group data of mean arterial pressure and heart rate response to ICV high-Na aCSF infusion in Sham-4 and AB-4. *$P<0.05$ vs Sham (n=3 in each group).

or Sham-R mice. There were no significant differences in arterial pressure and heart rate between the groups of Sham mice (Online Table II).

Measurement in Awake Mice Using Radio-Telemetry System

In AB-4 mice (AB day 28), mean arterial pressure and heart rate were significantly higher than that in the mice before aortic banding. Furthermore, high salt intake (AB-H mice) dramatically increased mean arterial pressure to 171±5 mm Hg by day 35 after aortic banding (1 week after the starting high salt intake). The general conditions deteriorated in all AB-H mice, however, likely because of severe lung congestion (lung/body weight ratio, 7.0±0.1). In AB-R mice, mean arterial pressure increased mildly, and the highest mean arterial pressure value was 145±5 mm Hg on day 38 after aortic banding and thereafter gradually decreased to 124±7 mm Hg on day 56 after aortic banding (n=3 for each; see the online data supplement for details).

Salt Sensitivity in Sham Mice and AB Mice

High salt intake did not increase U-NE or U-E excretion in Sham mice (Figure 3A). In AB mice, however, high salt intake significantly increased U-NE and U-E excretion. Furthermore, U-NE excretion in AB mice began to increase within 5 days (AB-Hd5 mice) of beginning the high-salt diet (Figure 3A), although cardiac function was preserved (%FS 43±1%; n=5). ICV infusion of regular-Na aCSF did not significantly increase U-NE or U-E excretion in Sham mice or AB mice (Figure 3B). ICV infusion of high-Na aCSF significantly increased U-NE and U-E excretion in both Sham mice and AB mice. The increase in U-NE excretion in AB mice, however, tended to be greater than that in Sham mice ($P=0.1$), and the increase in U-E excretion was significantly greater in AB mice than in Sham mice (Figure 3B).

In the acute experiments, high-Na aCSF ICV infusion increased arterial pressure and heart rate in both Sham-4 mice and AB-4 mice, but the degree of these changes was significantly greater in AB-4 mice (Figure 3C). The pressor response to angiotensin II ICV infusion was greater in AB-4 mice than Sham-4 mice (ΔMAP 8.6±1.2 mm Hg in Sham-4, 22.3±3.4 mm Hg in AB-4 mice, n=4 for each), however, the pressor response to carbachol ICV infusion did not differ between groups (ΔMAP: 9.5±1.8 mm Hg in Sham-4, 13.7±1.5 mm Hg in AB-4 mice; n=4 for each).

Na concentration in the brain tissues (circumventricular tissues including hypothalamus) was higher in AB-H mice than in the other groups (AB-H, 116±2 ppm; AB-R, 102±4 ppm; Sham-R, 104±2 ppm; Sham-H, 104±2 ppm; n=5 for each; $P<0.05$).

Effects of High-Na aCSF ICV Infusion on Cardiac Function

In AB mice, high-Na aCSF ICV infusion significantly increased LVDD (3.4±0.4 mm) and decreased %FS (32±1%) compared with regular-Na aCSF ICV infusion (LVDD, 3.2±0.5 mm; %FS, 41±1%; n=5 for each; $P<0.05$). Arterial pressure did not differ between AB mice with high-Na aCSF and regular-Na aCSF (94±3 mm Hg in high-Na aCSF,

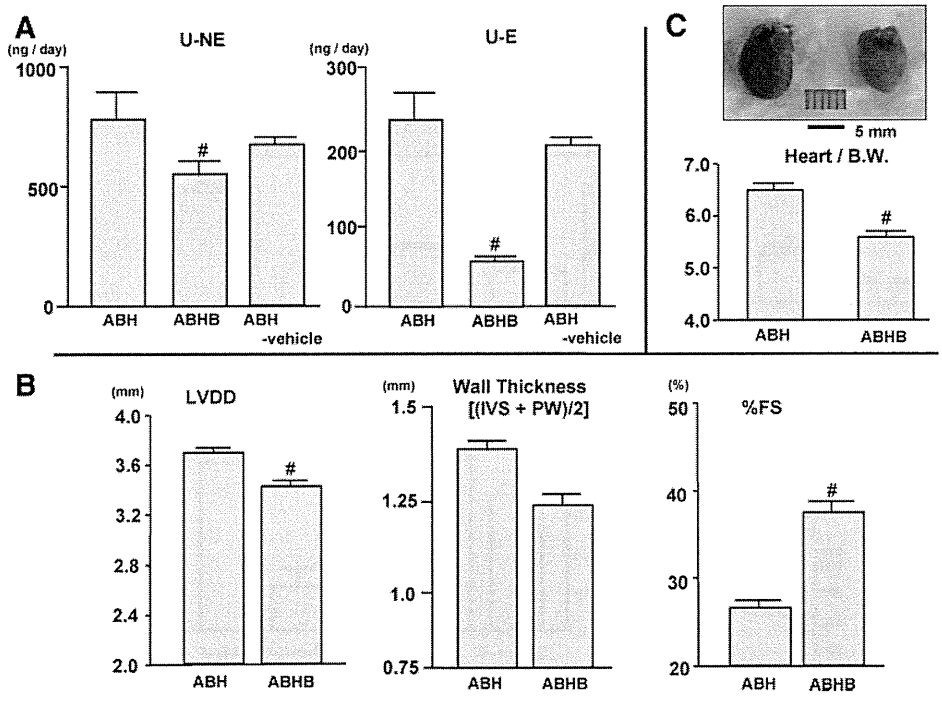

Figure 4. A, The 24-hour U-NE and U-E excretion in each group after ICV benzamil (AB-HB) infusion. #$P<0.05$ vs AB-H (n=5 to 10). B, Cardiac function evaluation by echocardiography in each group. IVS indicates interventricular septum; PW, posterior wall. #$P<0.05$ vs AB-H (n=8 in each group). C, Relative heart weight in each group. #$P<0.05$ vs AB-H (n=6 in each group).

101±5 mm Hg in regular-Na aCSF; n=4 for each). In Sham mice, high-Na aCSF ICV infusion had no significant effects on cardiac function compared with regular-Na aCSF ICV infusion (LVDD, 3.1±0.2 mm in high-Na aCSF versus 3.1±0.3 mm in regular-Na aCSF; %FS, 46±2% in high-Na aCSF versus 48±3% in regular-Na aCSF; n=5 for each).

Effects of ENaC Blocker ICV Infusion on Cardiac Function

In comparison with AB-H mice, ICV infusion of the ENaC blocker benzamil (AB-HB mice) significantly decreased U-NE and U-E excretion (Figure 4A). Cardiac function (LVDD and %FS) significantly improved in AB-HB mice compared with AB-H mice (Figure 4B). Relative heart weight decreased in AB-HB mice compared with AB-H mice (Figure 4C). Arterial pressure was significantly higher and heart rate was lower in AB-HB mice than in AB-H mice (Online Table II). ICV infusion of benzamil did not affect these measures in AB-R mice, and ICV infusion of vehicle in AB-H mice also did not significantly decrease U-NE and U-E excretion (data not shown).

Rho-Kinase Activity and AT_1R Expression in the Brain

The amount of AT_1R and the expression of p-moesin, a substrate of Rho-kinase, in the brain stem and circumventricular tissue were significantly higher in AB-4 mice than in Sham-4 mice (Figure 5).

Effects of ICV Infusion of Rho-Kinase Inhibitor and AT_1R Blocker on Cardiac Function

In comparison with AB-H mice, ICV infusion of the Rho-kinase inhibitor Y-27632 (AB-HY mice) or AT_1R blocker telmisartan (AB-HT mice) induced a significant decrease in U-NE and U-E excretion (Figure 6A). In AB-HT mice, U-NE and U-E decreased in a dose-related manner. Cardiac function was also significantly improved in AB-HY mice or AB-HT mice compared with AB-H mice (Figure 6B). Relative heart weight was decreased in AB-HY mice or AB-HT mice compared with AB-H mice (Figure 6C). Heart rate was significantly decreased in AB-HY mice or AB-HT mice compared with AB-H mice (Online Table II). Infusion of vehicle (aCSF or DMSO) did not have these effects.

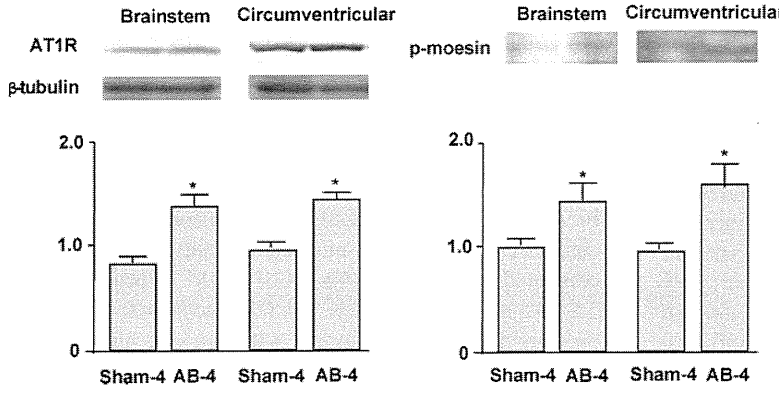

Figure 5. Left, Representative Western blots demonstrating the expression of AT_1R in the brain (circumventricular tissues including hypothalamus and brain stem tissues) of Sham-4 or AB-4. The graph shows the means for the quantification of 4 separate experiments. Data are expressed as the relative ratio to β-tubulin expression (n=4 in each group). *$P<0.05$ vs Sham-4. Right, Representative Western blot demonstrating the expression of p-moesin, a substrate of Rho-kinase in the brain (circumventricular tissues including hypothalamus and brain stem tissues) of Sham-4 or AB-4. The graph shows the means for the quantification of 3 separate experiments. Data are expressed as the relative ratio to Sham-4, which was assigned a value of 1 (n=3 in each group). *$P<0.05$ vs Sham.

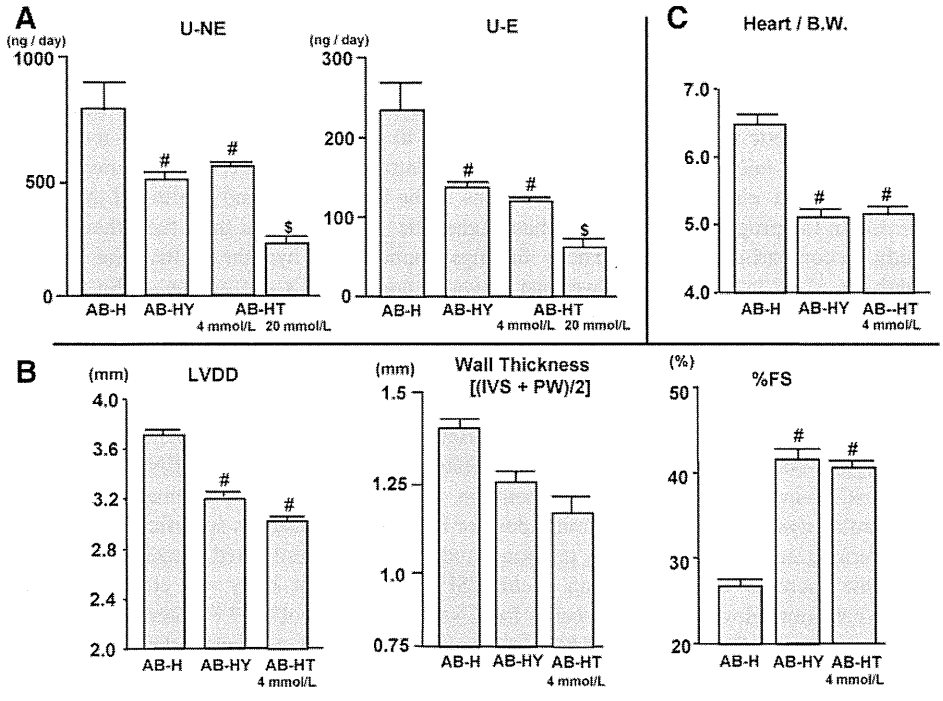

Figure 6. A, The 24-hour U-NE and U-E excretion in each group after Y-27632 (AB-HY) or telmisartan (AB-HT) ICV infusion. #$P<0.05$ vs AB-H (n=5 to 10), \$$P<0.05$ vs AB-HT 4 mmol/L. B, Cardiac function evaluation by echocardiography in each group after Y-27632 (AB-HY) or telmisartan (AB-HT) ICV infusion. IVS indicates interventricular septum; PW, posterior wall. #$P<0.05$ vs AB-H (n=5 to 8). C, Relative heart weight in each group after Y-27632 (AB-HY) or telmisartan (AB-HT) ICV infusion. #$P<0.05$ vs AB-H (n=5 to 6).

Serum Parameters

Serum Na concentration did not differ between groups (Sham-4, 151±2 mEq/L; AB-4, 151±1 mEq/L; AB-R, 150±1 mEq/L; AB-H, 152±1 mEq/L). Serum creatinine concentration, as a marker of renal function, also did not differ between groups (Sham-4, 0.11±0.01 mg/dL; AB-4, 0.09±0.01 mg/dL; AB-R, 0.12±0.01 mg/dL; AB-H, 0.11±0.01 mg/dL). Serum aldosterone levels were not different between Sham-4 and AB-4 mice and were significantly lower in AB-H mice than in AB-4 mice, AB-R mice, and Sham-4 mice (Sham-4, 120±11 pg/dL; AB-4, 145±28 pg/dL; AB-R, 163±17 pg/dL; AB-H, 54±6 pg/dL; n=6 to 7; $P<0.05$).

Discussion

The major findings of the present study were that mice with pressure overload produced by aortic banding acquired brain Na sensitivity via the activation of brain ENaCs through stimulation of the Rho/Rho-kinase pathway and RAS. Because of the acquired brain Na sensitivity, high salt intake led to sympathetic activation, which led to the deterioration of cardiac function. These findings are novel and suggest new targets for studies of the prevention and treatment of cardiac deterioration in patients with pressure overload, such as hypertensive heart disease.

The most important finding of the present study was that the mice with pressure overload acquired brain Na sensitivity and a high-salt diet increased the sympathetic outflow before cardiac dysfunction was detected. In AB-4 mice, only LVWT tended to increase compared to the Sham-4 mice, but there was no effect on cardiac function. Both a high-salt and regular-salt diet for an additional 4 weeks, however, induced cardiac dysfunction in AB mice compared with Sham mice. Furthermore, AB mice on the high-salt diet exhibited significantly more severe cardiac dysfunction and greater activation of the sympathetic system than AB mice on the regular-salt diet. This high-salt induced enhanced sympathetic drive was obvious before cardiac function was impaired. In Sham mice, a high salt intake did not increase U-NE and U-E excretion and had no effect on cardiac function. These results strongly suggest that the mice with pressure overload acquired the salt sensitivity before cardiac function began to deteriorate and that a high salt intake augmented cardiac dysfunction by inducing sympathetic activation.

To clarify the contribution of central mechanisms to the acquisition of salt sensitivity in mice with pressure overload, we examined the effects of high-Na in the CSF on sympathetic activity and arterial pressure after ICV infusion of high-Na or regular-Na aCSF. Compared with ICV infusion of regular-Na aCSF, high-Na aCSF induced significant increases in U-NE and U-E excretion in both groups of mice. The increased U-NE excretion in AB mice, however, tended to be greater than that in Sham mice ($P=0.1$), and the increase in U-E excretion was significantly greater in AB mice than in Sham mice. Furthermore, ICV infusion of high-Na aCSF induced significantly greater increases in arterial pressure and heart rate in AB-4 mice than in Sham-4 mice. To assess the specificity of the pressure response to a high-Na ICV infusion, we examined the response to other central stimuli, such as angiotensin II and carbachol. The response to angiotensin II was greater in AB-4 mice than Sham-4 mice. In contrast, the response to carbachol was not different between groups. The effect of the angiotensin II ICV infusion was supported by the findings that the extent of brain AT_1R was greater in AB-4 mice than Sham-4 mice, and the effect of carbachol ICV infusion indicated the specific activation of the brain RAS and Na sensing system. Together with the findings from the systemic salt loading, our findings suggest that the acquisition of Na sensitivity in the brain of

mice with pressure overload results from two different mechanisms: (1) the enhancement of Na uptake into the brain and (2) the increase in responsiveness to Na within the brain.

Another important finding of the present study was the high-Na aCSF-induced activation of the sympathetic system, which further deteriorates cardiac function in mice with pressure overload. There are some reports that enhanced sympathetic drive plays an important role in the progression of heart failure.[20,21] In the present study, in comparison with ICV infusion of regular-Na aCSF, high-Na aCSF induced a significant decline in cardiac function. To evaluate the possibility that the increase in the afterload induced by increased arterial pressure affected cardiac function, we measured arterial pressure 2 weeks after ICV infusion of high-Na aCSF and confirmed that arterial pressure did not significantly increase compared with regular-Na ICV infusion. These results suggest that high-Na aCSF-induced sympathetic hyperactivation may lead to cardiac dysfunction in mice with pressure overload and the deterioration of cardiac function may not be attributable to the increase in the afterload induced by the arterial pressure elevation. However, high-salt loading caused further decreases in cardiac function in AB mice, indicating that high-salt loading may induce further decrease in cardiac function both by sympathetic activation and an increase in arterial pressure in AB mice.

Arterial pressure in AB-4 mice was significantly higher than that in Sham-4 mice; and arterial pressure in AB-H 1-week mice, which were loaded with a high-salt diet for 1 week, was further increased compared with that in AB-4 mice. Arterial pressure in AB-R mice and AB-H mice decreased to levels similar or lower than that in Sham mice within 8 weeks. This may relate to cardiac dysfunction. In fact, the LVEDP in AB-H mice was significantly greater than that in AB-R or Sham-R mice and the LV %FS in AB-H mice was significantly smaller than that in AB-R or Sham-R mice. To validate the arterial pressure measurements, we measured arterial pressure and heart rate using a radio-telemetry system with mice in the awake state. At day 28 after aortic banding (AB-4 mice), arterial pressure was significantly higher than that before aortic banding. Thereafter, in AB-H mice, arterial pressure was significantly further increased at day 35 (1 week after the starting high-salt diet), but the general health of the mice deteriorated, likely because of severe lung congestion, which was supported by the high lung/body weight ratio. In AB-R mice, arterial pressure peaked at around day 40 and then gradually decreased. Implantation of the telemetry catheter in the carotid artery might further augment the pressure overload and induce severe lung congestion in AB-H mice. Therefore, we examined the arterial pressure under anesthesia in acute experiments. The findings indicate that aortic banding causes a pressure overload for LV and high-salt loading superimposed on aortic banding further augments the pressure overload.

To explore the mechanisms of the acquisition of brain Na sensitivity, we examined the effects of an ENaC blocker, benzamil. Brain ENaCs are involved in the high salt–induced increase in central sympathetic outflow in salt-sensitive hypertensive rats.[1,3] In the present study, brain ENaC blockade by benzamil attenuated the high salt–induced activation of the sympathetic nervous system and the deterioration of cardiac function. Furthermore, we examined the brain Na concentrations in each group. We were unable to measure Na concentrations in the CSF in the present study, because in mice it is difficult to obtain the volume of CSF required to measure Na concentration. Therefore, we measured the Na concentrations in the brain tissues and confirmed that AB-H mice had higher Na concentrations than the other groups. These findings support our hypothesis that the pressure overload activates brain ENaCs and augments Na transport from plasma to the CSF, resulting in sympathoexcitation. However, we did not examine the effects of brain ENaCs on Na transport directly and ENaCs have both epithelial and neural components.[11] Therefore, it is possible that the benzamil may affect ENaCs on neural components and cause sympathoinhibitory effects. The role of ENaCs on neural components in sympathetic modulation remains unclear. A similar dose of benzamil was used as specific ENaC blocker in previous studies,[4] and the estimated benzamil concentration in the CSF in the present study was considered to be specific for ENaCs ($<$100 nmol/L).[22–24] Therefore, the dose of benzamil used in the present study was adequate for use as a specific ENaC blocker. Further studies are required to measure ENaC activity directly. Although some studies have demonstrated that salt intake induces sympathoexcitation via central mechanisms[1–3] and the effects of brain ENaCs on cardiac function,[4] these previous studies used genetic models of salt-sensitive hypertension or heart failure induced by myocardial infarction, whereas we used the pressure overload produced by aortic banding model in mice without a genetic background of salt sensitivity.

Finally, we focused on Rho-kinase and angiotensin II as the mechanisms involved in brain ENaC activation in the mice with pressure overload, because ENaCs in kidney are reported to be activated by Rho-kinase[12] and angiotensin II.[13] In addition, we recently reported that Rho-kinase[16,25–27] and angiotensin II[28] in the brain contribute to cardiovascular regulation via the sympathetic nervous system. In the present study, we confirmed that compared to Sham-4 mice, the brains of AB-4 mice had higher levels of AT_1R and higher Rho-kinase activity, and blockade of either AT_1R or Rho-kinase attenuates high salt–induced sympathetic activation and cardiac dysfunction. These findings suggest that enhanced brain Na sensitivity results from the activation of brain ENaCs via the Rho/Rho-kinase pathway and RAS in mice with pressure overload. However, ENaCs may be upstream of RAS in brain.[29] In the present study, we did not address this issue. Further studies are needed to clarify the relationship between RAS and ENaCs in brain. It is possible that renal blood flow is reduced in mice with suprarenal abdominal aortic banding, resulting in renal dysfunction[30] concomitant with activation of the systemic RAS.[31] It is unlikely that this occurred in the present study because we confirmed that serum creatinine and aldosterone levels were not significantly different between groups and the mean arterial pressure in the AB-4 mice measured from the right femoral artery was above 90 mm Hg, suggesting that the aortic banding procedure did not significantly reduce renal blood flow and impair renal function. Previous studies